Electronic Research Archive

https://www.aimspress.com/journal/era

ERA, 32(6): 4043–4073.
DOI: 10.3934/era.2024182
Received: 11 April 2024
Revised: 30 May 2024
Accepted: 14 June 2024
Published: 24 June 2024

Research article

Modified fractional order social media addiction modeling and sliding mode control considering a professionally operating population

Ning Li* **and Yuequn Gao**

College of Sciences, Northeastern University, Shenyang 110819, China

* **Correspondence:** Email: lining80@163.com.

Abstract: With the advancement of technology, social media has become an integral part of people's daily lives. This has resulted in the emergence of a new group of individuals known as "professional operation people". These individuals actively engage with social media platforms, taking on roles as content creators, influencers, or professionals utilizing social media for marketing and networking purposes. Therefore, in this article, we designed a six-dimensional fractional-order social media addiction model (FOSMA) in the sense of Caputo, which took into account the professional operations population. Initially, we established the positivity and boundedness of the FOSMA model. After that, the basic regeneration number and the equilibrium points (no addiction equilibrium point and addiction equilibrium point) were computed. Then, the local asymptotic stability of the equilibrium points were proved. In order to investigate the bifurcation behavior of the model when $R_0 = 1$, we extended the Sotomayor theorem from integer-order to fractional-order systems. Next, by the frequency analysis method, we converted the fractional order model into an equivalent partial differential system. The tanh function was introduced into the scheme of sliding mode surface. The elimination of addiction was achieved by the action of the fractional order sliding mode control law. Finally, simulation results showed that fractional order values, nonlinear transmission rates, and specialized operating populations had a significant impact on predicting and controlling addiction. The fractional-order sliding mode control we designed played an important role in eliminating chatter, controlling addiction, and ensuring long-term effectiveness. The results of this paper have far-reaching implications for future work on modeling and control of fractional-order systems in different scenarios, such as epidemic spread, ecosystem stabilization, and game addiction.

Keywords: fractional order model; professional operating population; nonlinear incidence; forward bifurcation; fractional order sliding mode control; sliding mode surfaces

1. Introduction

With the development of technology, the forms and types of social media (SM) are colorful and complex, such as Facebook, Twitter, Instagram, etc. Social media are bringing great convenience to people's lives, and these advantages include information sharing and communication, teamwork and working from home, data sharing, sharing equipment and peripherals, services, and education [1–3]. However, it raises concerns. Numerous studies have shown that social media addiction can lead to many negative effects, including depression, worry, anxiety, mental discomfort, and academic decline [4–6]. In particular, during the COVID-19 pandemic, people were isolated in their homes and relied heavily on social media, which not only led to addiction, but also to anxiety [7]. This indicates an urgent need to investigate the spreading mechanisms of social media addiction and to develop effective control measures.

Mathematical modeling has achieved outstanding results in many areas, such as addiction modeling [8–12], infectious disease modeling [13–19], and ecosystem modeling [20–22]. Therefore, it is essential that we use mathematical modeling to study the transmission mechanisms of social media addiction (SMA). We can apply the SIR model from infectious disease dynamics to the study of SMA. The reason is that the mechanism of transmission of infectious diseases is from infected individuals to healthy individuals through contact, which is the same as the mechanism of transmission from addicted individuals to healthy individuals through contact. Recently, results have been achieved in mathematical modeling of SMA mechanisms by applying the SIR model [23, 24]. In [24], Alemneh et al. developed a 5-dimensional integer-order SMA model and designed optimal controls to decay the SMA propagation.

With the continuous improvement and development of fractional calculus, detailed results on fractional-order social media addiction modeling can be found in [25–30]. For example, Maayah et al. used the Caputo differential operator to study the Hilbert approximate solutions of the SMA model and the geometric behavior of fractions [25]. Kongson et al. modeled SMA using the Atangana-Baleanu-Caputo type derivative and proposed a numerical simulation technique to solve the model [26]. Rashid et al. modeled SMA using fractal-fractional order derivatives. Detailed answers are given on fractional order effects and numerical simulation techniques [27]. Momani et al. considered fractional order calculus with singular kernels and fractal-fractional operators to study SMA models [28]. Malik et al. explored the fractional-order SMA mathematical model, which was interpreted by applying the q-homology analysis Sumudu transformation method [29]. We utilize Caputo type fractional order derivatives to model the propagation of SMA. This is because the Caputo type fractional order model has the same initial conditions as the integer order model and its constant derivative is 0. In addition, the fractional order model will make the dynamical behavior of the model more complex [31, 32].

As the market expands, social media is becoming more commercialized and standardized. This has directly led to the emergence of professionals specializing in social media operations, such as social media experts and social media marketers. During the process of social media addiction, groups professionally engaged in social media dissemination influence users' social media usage habits and frequency by spreading content through social media, which may indirectly cause healthy individuals to become dependent on social media. Their activities include creating appealing content, encouraging user interaction, and enhancing user engagement with social media through various means [33, 34]. This is consistent with the introduced professional population in [12]. To study the spread of social

media addiction in the real world, unlike previous literature, we for the first time introduce a type of population, namely, the professionally operated population (marketing population), into the model of social media addiction. This not only greatly enriches the realism of the model, but also makes the dynamical behavior of the model more complex.

Similar to the multiple forms of incidence in infectious diseases [35–40], we also introduce nonlinear transmission rates in our model of social media addiction. Due to a large increase in the population with addiction or conscious protective measures by the healthy population, the valid contact rate between the addicted population and the healthy population may reach saturation at high levels of transmission. If the addiction population increases, the transmission rate decreases, which can be used to explain the "psychological" effect [41,42], that when there is a large number of addicted people, the transmission power may decrease. This is because in the presence of a high number of addicts, people may be inclined to reduce their contact with them, to actively and consciously restrain themselves from social media, or to adopt a strict upbringing in the family.

Designing appropriate controllers to control the spread of addiction is a crucial part of the process. Here, we design a fractional order sliding mode control that can eliminate addiction in a finite time. This approach is chosen because classical integer order sliding mode control exhibits high frequency chattering and the conventional controllers do not ensure fast convergence of the system [43,44]. Additionally, sliding mode control based on fractional order calculus can offer better properties for the control system, such as robustness and convergence. However, fractional order sliding mode controls have primarily been used for chaos control in fractional order systems [43,45–47]. Dadras et al. design sliding mode controllers for fractional order chaotic financial systems, ensuring robustness to system uncertainty and asymptotic stability under external disturbances [47]. Recently, researchers have begun applying fractional-order sliding mode controllers to a wider range of scenarios [48–51]. For example, Boonyaprapasorn et al. introduced fractional-order sliding mode controllers for fractional-order HBV epidemic models to control susceptible and infected populations at desired levels, reducing the occurrence of chattering [48]. Pourhashemi et al. proposed two new fractional sliding mode surfaces, achieving stabilization with/without uncertainty and external disturbances by designing fractional sliding mode controls. These controls are applied to fractional order nonlinear biological systems for further study [50]. Borah et al. studied six fractional order models of chaotic diseases, designing and analyzing suitable fractional order sliding mode controllers to control chaos in biomathematical models that require stability and anti-controllers to generate chaos where there was none [51].

Inspired by the above viewpoints, we innovatively proposed a 6-dimensional fractional-order designed media addiction model (FOSMA). The following are the major contributions.

1) For the first time, we incorporated groups that professionally operate social media into the SMA model, correcting the fractional-order dimension mismatch problem and examining the influence of these groups on the model's dynamic behavior. 2) To investigate bifurcation behavior, we generalized the Sotomayor theorem from integer-order models to fractional-order systems. 3) For the first time, we applied fractional-order sliding mode control to fractional-order social media addiction. We introduced a novel frequency distribution model, converting the fractional-order model into an equivalent partial differential model. Furthermore, we designed a new fractional-order sliding mode surface. It has been demonstrated that fractional-order sliding mode control converges in finite time, significantly reducing chattering and aiding in addiction elimination.

The rest of the article is summarized as follows. In Section 2, we provide the fundamentals. In

Section 3, we construct the FOSMA model and discuss its positivity and boundedness of the model. In Section 4, we compute the basic regeneration number and the equilibrium point, study the stability of the equilibrium point, and analyze the generation of bifurcations. In Section 5, we transform the fractional order system into a partial differential equation model. Moreover, we design the fractional order sliding mode surface and give the fractional order sliding mode control law. The numerical simulation results are given in Section 6 to verify the correctness of our conclusions. Finally, the results of this paper are summarized.

2. Basic knowledge

First, we introduce the basics of the article.

Definition 2.1. *[52, 53] The Caputo fractional order derivative for order $\alpha > 0$ is*

$$ {}_a\mathcal{D}_t^{\alpha} g(t) = \frac{1}{\Gamma(n-\alpha)} \int_a^t \frac{g^{(n)}(\tau)}{(t-\tau)^{\alpha-n+1}} d\tau, $$

where $g \in C^n([a,\infty), R)$, a is the initial moment, $t \geq a$, $\Gamma(.)$ is the gamma function and there exists $n \in Z^+$ such that $\alpha \in (n-1, n)$.

Remark 2.1. *$\Gamma(\cdot)$ is the Euler gamma function, which is defined as*

$$ \Gamma(z) = \int_0^{\infty} e^{-t} t^{z-1} dt, \ (\mathrm{Re}(z) > 0), \tag{2.1} $$

and the following equation holds

$$ \Gamma(z)\Gamma(1-z) = \frac{\pi}{\sin \pi z}, \ (0 < \mathrm{Re}(z) < 1). \tag{2.2} $$

Definition 2.2. *[52, 53] We give integrals of the Riemann-Liouville form:*

$$ {}_a\mathcal{I}_t^{\alpha} g(t) = {}_a\mathcal{D}_t^{-\alpha} g(t) = \frac{1}{\Gamma(\alpha)} \int_a^t \frac{g(\tau)}{(t-\tau)^{1-\alpha}} d\tau, \ g(t) \in \mathcal{L}^1([a,T]), \tag{2.3} $$

where $\mathcal{L}^1$ is the set of the Lebesgue integrable function, $\alpha > 0$, a is the starting point.

Theorem 2.1. *[52, 53] If $g(t)$ is continuously derivable of order n and ${}_a\mathcal{D}_t^{\alpha} g(t)$ is continuous piecewise on $[a,\infty)$ while there exists $a > 0$, $n-1 < a < n$, $n \in N$, then its Laplace transform is*

$$ L({}_a\mathcal{D}_t^{\alpha} g(t), s) = \int_0^{\infty} e^{-st} {}_a\mathcal{D}_t^{\alpha} g(t) dt = s^{\alpha} G(s) - \sum_{k=0}^{n-1} s^{\alpha-k-1} g^{(k)}(0); n-1 \leq \alpha \leq n, $$

where $G(s) = L({}_a\mathcal{D}_t^{\alpha} g(t), s)$.

Theorem 2.2. *[52, 53] The two-parameter form of the Mittag-Leffler function is $E_{\alpha,\beta}(z) = \sum_{k=0}^{\infty} \frac{z^k}{\Gamma(\alpha k+\beta)}; (\alpha, \beta > 0)$; the one-parameter form is $E_{\alpha,1}(z) = \sum_{k=0}^{\infty} \frac{z^k}{\Gamma(\alpha k+1)} = E_1(z)$. For any $\lambda \in C$ and $m, n > 0$, it will have the following formula*

$$ L(x^{n-1} E_{m,n}(-\lambda x^m)) = \frac{s^{m-n}}{s^m + \lambda}, $$

for $\mathrm{Re}(x) > \|\lambda\|^{\frac{1}{m}}$, where $\mathrm{Re}(x)$ represents the real part of the imaginary number x.

Theorem 2.3. *[52, 53] If $m, n > 0$ and $x \in C$, then*

$$E_{m,n}(x) = xE_{m,m+n}(x) + \frac{1}{\Gamma(n)}.$$

Theorem 2.4. *[52, 53] The equilibrium point E^* is locally asymptotically stable if all eigenvalues $\lambda_i (i = 1, 2, ... n)$ of the Jacobi matrix $\mathcal{J} = \frac{\partial g}{\partial x}$, where $g = [g_1, g_2 ... g_n]^T$, computed at E^*, satisfy $\left|\arg(\lambda_i)\right| > \alpha\frac{\pi}{2},\ i = 1, 2, ... n$.*

Remark 2.2. *It is mentioned in [52] that exponential stability cannot be applied to prove the asymptotic stability of fractional order model. Therefore, it is proposed that the state vector decays slowly with $t^{-\alpha}$ to the equilibrium point, and it is this phenomenon that results in fractional systems with long memory effects, where this power law stability $t^{-\alpha}$ is a particular case of Mittag-Leffler stability.*

3. FOSMA model

First, we give a modified fractional order social media addiction model. We assume that the population is homogeneously mixed, meaning that everyone has an equal chance of interacting with others. This is easy to analyze and understand, providing quick estimates of addiction trends.

If the fractional order differential operator is directly added to the left end of the integer order model as in [27], we find that the dimensions of the equations are inconsistent at both ends. Since the dimension of the left side of the equation is $-\alpha$ and the dimension of the right side is -1, we adjust the non-negative parameter of the right side of the equation to be a α-exponent to balance out the inconsistency in dimension. We propose the following equation:

$$\begin{aligned}
{}_0^C\mathcal{D}_t^{\alpha} S(t) &= \Pi^{\alpha} - \frac{\beta_1^{\alpha}\sigma_1^{\alpha} A(t)S(t)}{1 + aA(t)} - \frac{\beta_2^{\alpha}\sigma_2^{\alpha} P(t)S(t)}{1 + bP(t)} - (\mu^{\alpha} + \delta^{\alpha})S(t) + \gamma_2^{\alpha} R(t);\\
{}_0^C\mathcal{D}_t^{\alpha} E(t) &= \frac{\beta_1^{\alpha}\sigma_1^{\alpha} A(t)S(t)}{1 + aA(t)} + \frac{\beta_2^{\alpha}\sigma_2^{\alpha} P(t)S(t)}{1 + bP(t)} - (\alpha_1^{\alpha} + \alpha_2^{\alpha} + \alpha_3^{\alpha} + \mu^{\alpha})E(t);\\
{}_0^C\mathcal{D}_t^{\alpha} A(t) &= \alpha_1^{\alpha} E(t) - (\mu^{\alpha} + \nu^{\alpha} + \lambda^{\alpha} + \omega^{\alpha})A(t);\\
{}_0^C\mathcal{D}_t^{\alpha} P(t) &= \alpha_2^{\alpha} E(t) + \omega^{\alpha} A(t) - (\mu^{\alpha} + \theta^{\alpha})P(t);\\
{}_0^C\mathcal{D}_t^{\alpha} R(t) &= \alpha_3^{\alpha} E(t) + \lambda^{\alpha} A(t) + \theta^{\alpha} P(t) - (\mu^{\alpha} + {\gamma_1}^{\alpha} + {\gamma_2}^{\alpha})R(t);\\
{}_0^C\mathcal{D}_t^{\alpha} Q(t) &= \delta^{\alpha} S(t) + \gamma_1^{\alpha} R(t) - \mu^{\alpha} Q(t).
\end{aligned} \tag{3.1}$$

The initial conditions of model (3.1) are

$$S(0) \geq 0, E(0) \geq 0, A(0) \geq 0, P(0) \geq 0, R(0) \geq 0, Q(0) \geq 0. \tag{3.2}$$

The parameters in the model (3.1) are non-negative and their actual practical significance is shown in Table 1. The flow chart of the model (3.1) is shown in Figure 1.

Table 1. practical significance of parameters in the FOSMA model (3.1).

Parameter	Practical significance
Π	Recruitment rates of $S(t)$
β_1	The rate of infection of $S(t)$ by $A(t)$
σ_1	The rate of contact between the $A(t)$ and the $S(t)$
a	The rate of suppression of transmission from the $A(t)$
β_2	The rate of infection of $S(t)$ by $P(t)$
σ_2	The rate of contact between $P(t)$; and $S(t)$
b	The rate of suppression of transmission from the $P(t)$
μ	Natural mortality rate
δ	The rate of transfer from the $S(t)$ to the $Q(t)$
γ_2	The rate of transfer from the $R(t)$ to the $S(t)$
α_1	The rate of transfer from the $E(t)$ to the $A(t)$
α_2	The rate of transfer from the $E(t)$ to the $P(t)$
α_3	The rate of transfer from the $E(t)$ to the $R(t)$
ν	Mortality rates for overuse of SM
λ	The rate of transfer from the $A(t)$ to the $R(t)$
ω	The rate of transfer from the $A(t)$ to the $P(t)$
θ	The rate of transfer from the $P(t)$ to the $R(t)$
γ_1	The rate of permanent SM discontinuation in the $R(t)$

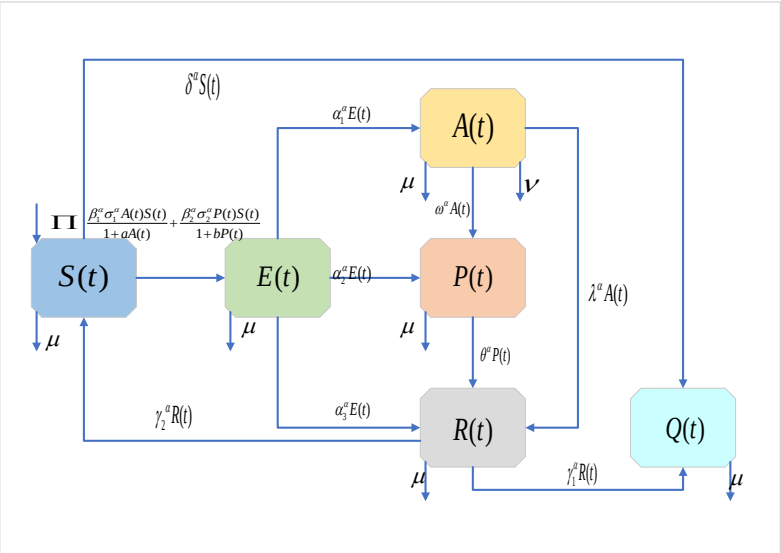

Figure 1. Flow chart of FOSMA model (3.1).

In the FOSMA model (3.1), $S(t)$ denotes the susceptible population, $E(t)$ represents the population that can develop addiction, $A(t)$ denotes the addicted population, $P(t)$ represents the population that operates social media professionally, $R(t)$ represents the recovered population, and $Q(t)$ stands for the population that permanently stops using social media.

Susceptible individuals $S(t)$ enter the system (3.1) at a recruitment rate of Π. They are infected by $A(t)$ and $P(t)$ at a non-linear transmission rate of $\frac{\beta_1\sigma_1 A(t)}{1+aA(t)} + \frac{\beta_2\sigma_2 P(t)}{1+bP(t)}$ into $E(t)$, and also enter ($Q(t)$) at a rate of δ. $E(t)$ will enter $A(t)$, ($P(t)$), and $R(t)$ at a rate of α_1, α_2, and α_3, respectively. $A(t)$ will enter $R(t)$ at a rate of λ and enter $P(t)$ at a rate of ω. $P(t)$ will enter $R(t)$ at a rate of θ. $R(t)$ will transition to $Q(t)$ at a rate of γ_1 and revert to $S(t)$ at a rate of γ_2. The natural mortality rate for each population is μ, and the addicted population will have a mortality rate of ν due to the overall decline in physical function that will result from overuse of SM.

The fundamental properties of the FOSMA model (3.1) solution are given next, which is to ensure that model (3.1) is practically meaningful. We give the existence uniqueness theorem for the solutions of the model (3.1).

Theorem 3.1. *For any non-negative initial condition (3.2), there is a unique solution of the FOSMA model (3.1).*

The method for proving this Theorem 3.1 is given in detail in [54] and is therefore omitted here. Immediately after, the positivity and boundedness of the FOSMA model (3.1) are given.

3.1. Positivity of the solution

Theorem 3.2. *The solution of FOSMA (3.1) is non-negative when the initial condition (3.2) is satisfied.*

Proof. By Π^α is a non-negative constant, so the following equation holds

$$ {}_0^C\mathcal{D}_t^{\alpha} S(t) \geq -(\mu^\alpha + \delta^\alpha) S(t). \tag{3.3}$$

The Laplace transform of Eq (3.3) is obtained

$$ \overline{S(s)} \geq \frac{s^{\alpha-1}}{s^{\alpha-1} + (\mu^\alpha + \delta^\alpha)} S(0). \tag{3.4}$$

By the conclusion in [55], the rewriting of Eq (3.4) yields

$$ S(t) \geq S(0) E_{\alpha,1}(-(\mu^\alpha + \delta^\alpha) t^\alpha) \geq 0; \ \forall t > 0. \tag{3.5}$$

We prove that the following equation also holds by the above way

$$\begin{aligned}
&E(t) \geq E(0) E_{\alpha,1}(-(\alpha_1^\alpha + \alpha_2^\alpha + \alpha_3^\alpha + \mu^\alpha) t^\alpha) \geq 0,\\
&A(t) \geq A(0) E_{\alpha,1}(-(\mu^\alpha + \nu^\alpha + \lambda^\alpha + \omega^\alpha) t^\alpha) \geq 0,\\
&P(t) \geq P(0) E_{\alpha,1}(-(\mu^\alpha + \theta^\alpha) t^\alpha) \geq 0,\\
&R(t) \geq R(0) E_{\alpha,1}(-(\mu^\alpha + \gamma_1^\alpha + \gamma_2^\alpha) t^\alpha) \geq 0,\\
&Q(t) \geq Q(0) E_{\alpha,1}(-\mu^\alpha t^\alpha) \geq 0. \forall t > 0.
\end{aligned}$$

Therefore, FOSMA (3.1) has a non-negative solution when condition (3.2) is satisfied.

3.2. Boundedness of the solution

Theorem 3.3. *When the initial condition (3.2) is in* $\Omega = \{(S, E, A, P, R, Q) \in \mathcal{R}_+^6,\ N(t) \leq N\}$, *where* $N = \max\{\frac{\Pi^\alpha}{\mu^\alpha},\ N(0)\}$, *then the solution of FOSMA (3.1) is also always in the set* Ω.

Proof. We let (S, E, A, P, R, Q) be the solution of FOSAM (3.1), then there will be $N = S + E + A + P + R + Q$.

Therefore, we have

$$\mathcal{D}_t{}^\alpha N(t) = \Pi^\alpha - \mu^\alpha N(t) - \nu^\alpha A(t) \leq \Pi^\alpha - \mu^\alpha N(t). \tag{3.6}$$

The Laplace transformation of Eq (3.6) yields

$$s^\alpha L(N(t)) - s^{\alpha-1}N(0) \leq \frac{\Pi^\alpha}{s} - \mu^\alpha L(N(t)). \tag{3.7}$$

After simplification, we get

$$L(N(t)) \leq \frac{\Pi^\alpha s^{-1}}{s^\alpha + \mu^\alpha} + \frac{s^{\alpha-1}}{s^\alpha + \mu^\alpha}N(0). \tag{3.8}$$

Next, using the Laplace inverse transform and the conclusion in [54] yields

$$\begin{aligned} N(t) &\leq \Pi t^\alpha E_{\alpha,\alpha+1}(-\mu^\alpha t^\alpha) + N(0)E_{\alpha,1}(-\mu^\alpha t^\alpha) \\ &\leq N(\mu^\alpha t^\alpha E_{\alpha,\alpha+1}(-\mu^\alpha t^\alpha) + E_{\alpha,1}(-\mu^\alpha t^\alpha)) \\ &= \frac{N}{\Gamma(1)}. \end{aligned}$$

Therefore $N(t)$ is bounded, then S, E, A, P, R, Q are also bounded.

At this point, we proved the feasibility of the model in a realistic sense. It lays the foundation for the next step of the analysis.

4. Stability analysis of equilibrium points

First, all possible equilibria of the FOSMA model (3.1) are derived theoretically and the basic regeneration number (R_0) is computed using the next generation matrix. Furthermore, the local asymptotic stability of all equilibrium points of the model (3.1) is proved. Finally, the bifurcation behavior at $R_0 = 1$ is proved by extending the Sotomayor's theorem for integer order systems to fractional order systems.

4.1. No addiction equilibrium (NAE)

For the FOSMA model (3.1), when there is no addicted population, i.e., $(E = A = P = R = 0)$. At this point, the NAE is expressed by the following equation

$$NAE = (S^0, E^0, A^0, P^0, R^0, Q^0) = (\frac{\Pi^\alpha}{\mu^\alpha + \delta^\alpha}, 0, 0, 0, 0, \frac{\delta^\alpha \Pi^\alpha}{\mu^\alpha(\mu^\alpha + \delta^\alpha)}).$$

Similar to the infectious disease model, the R_0 of the FOSMA model (3.1) represents the number of individuals infected by an addicted individual in a susceptible population. This calculation uses the same next generation matrix, as detailed in [54, 55]. $R_0 = \rho(FV^{-1})$, where, the infection matrice F and transfer matrice V are

$$F = \begin{pmatrix} 0 & \beta_1^\alpha \sigma_1^\alpha S^0 & \beta_2^\alpha \sigma_2^\alpha S^0 & 0 \\ 0 & 0 & 0 & 0 \\ 0 & 0 & 0 & 0 \\ 0 & 0 & 0 & 0 \end{pmatrix}, V = \begin{pmatrix} e_1 & 0 & 0 & 0 \\ -\alpha_1^\alpha & e_2 & 0 & 0 \\ -\alpha_2^\alpha & -\omega^\alpha & e_3 & 0 \\ -\alpha_3^\alpha & -\lambda^\alpha & -\theta^\alpha & e_4 \end{pmatrix},$$

where $e_1 = \alpha_1^\alpha + \alpha_2^\alpha + \alpha_3^\alpha + \mu^\alpha,\ e_2 = \mu^\alpha + \nu^\alpha + \lambda^\alpha + \omega^\alpha,\ e_3 = \mu^\alpha + \theta^\alpha,\ e_4 = \mu^\alpha + {\gamma_1}^\alpha + {\gamma_2}^\alpha$.

After simple calculations, we obtain

$$R_0 = \rho(FV^{-1}) = \frac{\alpha_1^\alpha}{e_1 e_2}(\beta_1^\alpha \sigma_1^\alpha \frac{\Pi^\alpha}{\mu^\alpha + \delta^\alpha} + \beta_2^\alpha \sigma_2^\alpha \frac{\Pi^\alpha}{\mu^\alpha + \delta^\alpha}(\frac{\alpha_1^\alpha \omega^\alpha + \alpha_2^\alpha e_2}{\alpha_1^\alpha e_3})). \tag{4.1}$$

Remark 4.1. *We can find that R_0 is composed of two parts: $R_0 = R_{01} + R_{02}$, $R_{01} = \frac{\alpha_1^\alpha}{e_1 e_2}\beta_1^\alpha \sigma_1^\alpha \frac{\Pi^\alpha}{\mu^\alpha + \delta^\alpha}$, $R_{02} = \frac{\alpha_1^\alpha}{e_1 e_2}\beta_2^\alpha \sigma_2^\alpha \frac{\Pi^\alpha}{\mu^\alpha + \delta^\alpha}(\frac{\alpha_1^\alpha \omega^\alpha + \alpha_2^\alpha e_2}{\alpha_1^\alpha e_3})$, where R_{01} represents the transmission from the addicted population to the susceptible population; R_{02} represents the transmission from the professional population to the susceptible population. Therefore, our introduction of $P(t)$ will make R_0 further increase compared to [26–29], which is also more realistic.*

4.2. Addiction equilibrium (AE)

Let the right end of the FOSMA model (3.1) be all zeros. After a simple calculation, we give the following theorem:

Theorem 4.1.

(i) For the FOSMA model (3.1), there always exists a no-addiction equilibrium point (NAE);

(ii) There exists a unique addiction equilibrium point (AE) for the FOSMA model (3.1) when $R_0 > 1$;

$$AE = (S^*, E^*, A^*, P^*, R^*, Q^*), \tag{4.2}$$

where $E^* = c_1 A^*,\ P^* = c_2 A^*,\ R^* = c_3 A^*,\ S^* = \frac{\Pi^\alpha}{\mu^\alpha + \delta^\alpha} - c_4 A^*; Q^* = \frac{\delta^\alpha \Pi^\alpha}{\mu^\alpha(\mu^\alpha + \delta^\alpha)} - c_5 A^*$ and $c_1 = \frac{e_2}{\alpha_1^\alpha},\ c_2 = \frac{\alpha_1^\alpha \omega^\alpha + \alpha_2^\alpha e_2}{\alpha_1^\alpha e_3},\ c_3 = \frac{\alpha_3^\alpha e_2 e_3 + \lambda^\alpha \alpha_1^\alpha e_3 + \theta^\alpha(\alpha_1^\alpha \omega^\alpha + \alpha_2^\alpha e_2)}{\alpha_1^\alpha e_3 e_4},\ c_4 = \frac{e_1 c_1 + \gamma_2^\alpha c_3}{\mu^\alpha + \delta^\alpha},\ c_5 = \frac{\gamma_1^\alpha c_3 - \delta^\alpha c_4}{\mu^\alpha}$.

Proof. Bringing addiction equilibrium point (AE) (4.2) into the first equation of the FOSMA model (3.1), a simplification leads to:

$$d_1 (A^*)^2 + d_2 A^* + d_3 = 0, \tag{4.3}$$

where

$$\begin{aligned} d_1 &= \beta_1^\alpha \sigma_1^\alpha b c_2 c_4 + \beta_2^\alpha \sigma_2^\alpha a c_2 c_4 + abc_2 c_4(\mu^\alpha + \delta^\alpha) + abc_2 \gamma_2^\alpha c_3, \\ d_2 &= \frac{c_2 \Pi^\alpha}{\mu^\alpha + \delta^\alpha}(\beta_2^\alpha \sigma_2^\alpha a - \beta_1^\alpha \sigma_1^\alpha b) + \beta_1^\alpha \sigma_1^\alpha c_4 + \beta_2^\alpha \sigma_2^\alpha c_2 c_4 + (2\gamma_2^\alpha c_3 + e_1 c_1), \\ d_3 &= \frac{e_1 e_2}{\alpha_1^\alpha} - \frac{\Pi^\alpha}{\mu^\alpha + \delta^\alpha}(\beta_1^\alpha \sigma_1^\alpha + \beta_2^\alpha \sigma_2^\alpha(\frac{\alpha_1^\alpha \omega^\alpha + \alpha_2^\alpha e_2}{\alpha_1^\alpha e_3})) = \frac{e_1 e_2}{\alpha_1^\alpha}(1 - R_0). \end{aligned}$$

We easily find that $d_1 > 0$, and when $R_0 > 1$, the relationship between the roots and coefficients of the quadratic equation shows that there exists a unique AE for the FOSMA model (3.1).

The stability of the fractional-order nonlinear model (3.1) is difficult to analyze, so we study the nonlinear model (3.1) using the linearization technique following the analytical method of the integer-order model. This is because the linear system can be accurately approximated as a substitute for the nonlinear system, and the difference between the two is negligible. We first analyze the local stability of NAE.

4.3. Stability analysis of NAE

The Jacobi matrix characterization matrix for model (3.1) at NAE is shown below:

$$\begin{pmatrix} s^\alpha + \mu^\alpha + \delta^\alpha & 0 & -\beta_1^\alpha \sigma_1^\alpha S^0 & -\beta_2^\alpha \sigma_2^\alpha S^0 & -\gamma_2^\alpha & 0 \\ 0 & s^\alpha + e_1 & \beta_1^\alpha \sigma_1^\alpha S^0 & \beta_2^\alpha \sigma_2^\alpha S^0 & 0 & 0 \\ 0 & -\alpha_1^\alpha & s^\alpha + e_2 & 0 & 0 & 0 \\ 0 & -\alpha_2^\alpha & -\omega^\alpha & s^\alpha + e_3 & 0 & 0 \\ 0 & -\alpha_3^\alpha & -\lambda^\alpha & -\theta^\alpha & s^\alpha + e_4 & 0 \\ -\delta^\alpha & 0 & 0 & 0 & -\gamma_1^\alpha & s^\alpha + \mu^\alpha \end{pmatrix}. \tag{4.4}$$

It can be easily found that the characteristic equation has three negative real roots, which are $-(\mu^\alpha + \delta^\alpha)$, $-\mu^\alpha$, $-e_4$.

Let $\chi = s^\alpha$. The characteristic equation of (4.4) reduces to

$$\chi^3 + f_1\chi^2 + f_2\chi + f_3 = 0, \tag{4.5}$$

where $f_1 = e_1 + e_2 + e_3$, $f_2 = e_1e_2 + e_1e_3 + e_2e_3 - \alpha_2^\alpha\beta_2^\alpha\sigma_2^\alpha S^0 - \alpha_1^\alpha\beta_1^\alpha\sigma_1^\alpha S^0$, $f_3 = e_1e_2e_3 - S^0(\alpha_1^\alpha\beta_1^\alpha\sigma_1^\alpha e_3 + \beta_2^\alpha\sigma_2^\alpha(\alpha_1^\alpha\omega^\alpha + \alpha_2 e_2)) = e_1e_2e_3(1 - R_0)$.

After that, we will have the following conclusion:

Theorem 4.2. *When the condition $R_0 < 1$ and $f_1f_2 > f_3$ are satisfied, the FOSMA model (3.1) is locally asymptotically stable at the NAE.*

Proof. We can find that $f_1 > 0$. When $R_0 < 1$, we will have $f_3 > 0$. Condition $f_1f_2 > f_3$ is also satisfied, then by the Routh–Hurwitz criterion [52, 53], the condition $\left|\arg(\chi_i)\right| > \frac{\alpha\pi}{2}$ is satisfied, the FOSMA model (3.1) is locally asymptotically stable at the NAE.

Next, similar to the approach used to analyze the stability around the NAE, we study the stability of the AE.

4.4. Stability analysis of AE

The characterization matrix of model (3.1) Jacobi matrix at AE is shown below:

$$\begin{pmatrix} s^\alpha + g_3 & 0 & g_4 & g_5 & -\gamma_2^\alpha & 0 \\ -(g_1 + g_2) & s^\alpha + e_1 & -g_4 & -g_5 & 0 & 0 \\ 0 & -\alpha_1^\alpha & s^\alpha + e_2 & 0 & 0 & 0 \\ 0 & -\alpha_2^\alpha & -\omega^\alpha & s^\alpha + e_3 & 0 & 0 \\ 0 & -\alpha_3^\alpha & -\lambda^\alpha & -\theta^\alpha & s^\alpha + e_4 & 0 \\ -\delta^\alpha & 0 & 0 & 0 & -\gamma_1^\alpha & s^\alpha + \mu^\alpha \end{pmatrix}, \tag{4.6}$$

where $g_1 = \frac{\beta_1^\alpha \sigma_1^\alpha A^*}{1+aA^*},\ g_2 = \frac{\beta_2^\alpha \sigma_2^\alpha P^*}{1+bP^*}, g_3 = \mu^\alpha + \delta^\alpha + g_1 + g_2,\ g_4 = \frac{\beta_1^\alpha \sigma_1^\alpha S^*}{(1+aA^*)^2},\ g_5 = \frac{\beta_2^\alpha \sigma_2^\alpha S^*}{(1+bP^*)^2}$.

It can be easily found that the characteristic equation has one negative real root, which is $-\mu^\alpha$. Let $\chi = s^\alpha$. The characteristic equation of (4.6) reduces to

$$\chi^5 + k_1\chi^4 + k_2\chi^3 + k_3\chi^2 + k_4\chi + k_5 = 0, \tag{4.7}$$

where $k_1 = f_1 + g_3 + e_4,\ k_2 = h_1 + f_1(g_3 + e_4) + g_3e_4,\ k_3 = h_2 + h_1(g_3 + e_4) + g_3e_4f_1 - \alpha_3^\alpha\gamma_2^\alpha(g_1 + g_2) + (g_1 + g_2)(\alpha_2^\alpha g_5 + \alpha_1^\alpha g_4),\ k_4 = h_2(g_3 + e_4) + g_3e_4h_1 - \gamma_2^\alpha(g_1 + g_2)(\alpha_3^\alpha(e_2 + e_3) + \alpha_2^\alpha\theta^\alpha + \alpha_1^\alpha\lambda^\alpha) + \alpha_1^\alpha\omega^\alpha g_5 + \alpha_1^\alpha e_3g_4 + \alpha_2^\alpha e_2g_5 + e_4(\alpha_2^\alpha g_5 + \alpha_1^\alpha g_4),\ k_5 = g_3e_4h_2 - (\alpha_1^\alpha\omega^\alpha\theta^\alpha + \alpha_2^\alpha\theta^\alpha e_2 + \alpha_2^\alpha\lambda^\alpha e_3) + e_4(\alpha_1^\alpha\omega^\alpha g_5 + \alpha_1^\alpha e_3g_4 + \alpha_2^\alpha e_2g_5)$. and $h_1 = e_1e_2 + e_1e_3 + e_2e_3 - \alpha_2^\alpha g_5 - \alpha_1^\alpha g_4,\ h_2 = e_1e_2e_3 - \alpha_1^\alpha\omega^\alpha g_5 - \alpha_1^\alpha e_3g_4 - \alpha_2^\alpha e_2g_5$.

We assume the following conditions

$$\mathbf{H1}: k_3 > 0,\ k_4 > 0,\ k_5 > 0. \tag{4.8}$$

$$\mathbf{H2}: \Delta_1 = \begin{vmatrix} k_1 & 1 \\ k_3 & k_2 \end{vmatrix} > 0,\ \Delta_2 = \begin{vmatrix} k_1 & 1 & 0 \\ k_3 & k_2 & k_1 \\ k_5 & k_4 & k_3 \end{vmatrix} > 0,\ \Delta_3 = \begin{vmatrix} k_1 & 1 & 0 & 0 \\ k_3 & k_2 & k_1 & 1 \\ k_5 & k_4 & k_3 & k_2 \\ 0 & 0 & k_5 & k_4 \end{vmatrix} > 0. \tag{4.9}$$

Then, we will have the following conclusion:

Theorem 4.3. *When the condition $R_0 > 1$,* **H1** *and* **H2** *are satisfied, the FOSMA model (3.1) is locally asymptotically stable at the AE.*

Proof. When the condition $R_0 > 1$, **H1** and **H2** are satisfied. By the Routh–Hurwitz criterion [52–55], we can obtain $\left|\arg(\chi_i)\right| > \frac{\alpha\pi}{2}$, the FOSMA model (3.1) is locally asymptotically stable at the AE.

4.5. Bifurcation analysis

From the dynamical point of view: as parameters are transformed, the state of the system may undergo abrupt changes or transitions. When a parameter reaches a certain threshold, the equilibrium point of the system changes from one to multiple (forward bifurcation). Alternatively, multiple equilibria merge into one or more new equilibria (backward bifurcation). Starting from real addiction scenarios: Addiction is also complicated by bifurcation behavior.

Classical integer-order systems have well-established theories about forward bifurcation or backward bifurcation, such as the central manifold theorem [56]. However, the theory of systems at fractional order is not yet perfect. Therefore, we draw on [27, 57] to study bifurcation in fractional order systems. We have the following conclusions for the FOSMA (3.1) model.

As expressed in the paper [27], the addiction-free equilibrium will lose its stability when $R_0 = 1$. When satisfying $f_2 \geq 0,\ f_1^2 \geq 4f_2$, the characteristic equation (4.5) will have two roots with negative real part and one zero root. Therefore, bifurcation behavior might occur at this point. The addicted population plays a decisive role in the propagation process, so we choose ${\beta_1}^\alpha = {\beta_1}^{\alpha*}$ as the bifurcation parameter. At this point, when $R_0 = \frac{{\alpha_1}^\alpha}{e_1e_2}\frac{\Pi^\alpha}{\mu^\alpha+\delta^\alpha}({\beta_1}^\alpha{\sigma_1}^\alpha + {\beta_2}^\alpha{\sigma_2}^\alpha(\frac{{\alpha_1}^\alpha\omega^\alpha+\alpha_2{}^\alpha e_2}{{\alpha_1}^\alpha e_3})) = 1$, we would have

$${\beta_1}^\alpha = {\beta_1}^{\alpha*} = \frac{1}{{\sigma_1}^\alpha}(\frac{e_1e_2e_3(\mu^\alpha + \delta^\alpha) - \Pi^\alpha{\beta_2}^\alpha{\sigma_2}^\alpha({\alpha_1}^\alpha\omega^\alpha + {\alpha_2}^\alpha e_2)}{\Pi^\alpha{\alpha_1}^\alpha e_3}). \tag{4.10}$$

When the eigenvalue of the eigenmatrix $\mathcal{J}^*(NAE)\big|_{\beta_1{}^\alpha=\beta_1{}^{\alpha*}}$ (4.4) is 0, we have

$$\mathcal{J}^*(NAE)\big|_{\beta_1{}^\alpha=\beta_1{}^{\alpha*}} = \begin{pmatrix} \mathcal{A}_3 & 0 & -\mathcal{A}_1 & -\mathcal{A}_2 & -\gamma_2{}^\alpha & 0 \\ 0 & e_1 & \mathcal{A}_1 & \mathcal{A}_2 & 0 & 0 \\ 0 & -\alpha_1{}^\alpha & e_2 & 0 & 0 & 0 \\ 0 & -\alpha_2{}^\alpha & -\omega^\alpha & e_3 & 0 & 0 \\ 0 & -\alpha_3{}^\alpha & -\lambda^\alpha & -\theta^\alpha & e_4 & 0 \\ -\delta^\alpha & 0 & 0 & 0 & -\gamma_1{}^\alpha & \mu^\alpha \end{pmatrix}, \tag{4.11}$$

where $\mathcal{A}_1 = \beta_1{}^\alpha\sigma_1{}^\alpha\frac{\Pi^\alpha}{\mu^\alpha+\delta^\alpha}$, $\mathcal{A}_2 = \beta_2{}^\alpha\sigma_2{}^\alpha\frac{\Pi^\alpha}{\mu^\alpha+\delta^\alpha}$, $\mathcal{A}_3 = \mu^\alpha + \delta^\alpha$.

Next, the left and right eigenvectors of the matrix (4.11) are computed. Let the right eigenvector be $\tau = (\tau_1, \tau_2, \tau_3, \tau_4, \tau_5, \tau_6)^T$ and the left eigenvector be $\rho = (\rho_1, \rho_2, \rho_3, \rho_4, \rho_5, \rho_6)$. We have $\mathcal{J}^*(NAE)\tau = 0, \mathcal{J}^{*T}(NAE)\rho = 0$. where

$$\begin{cases} \mathcal{A}_3\tau_1 - \mathcal{A}_1\tau_3 - \mathcal{A}_2\tau_4 - \gamma_2{}^\alpha\tau_5 = 0, \\ e_1\tau_2 + \mathcal{A}_1\tau_3 + \mathcal{A}_2\tau_4 = 0, \\ -\alpha_1{}^\alpha\tau_2 + e_2\tau_3 = 0, \\ -\alpha_2{}^\alpha\tau_2 - \omega^\alpha\tau_3 + e_3\tau_4 = 0, \\ -\alpha_3{}^\alpha\tau_2 - \lambda^\alpha\tau_3 - \theta^\alpha\tau_4 + e_4\tau_5 = 0, \\ -\delta^\alpha\tau_1 - \gamma_1{}^\alpha\tau_5 + \mu^\alpha\tau_6 = 0. \end{cases} \quad \begin{cases} \mathcal{A}_3\rho_1 - \delta^\alpha\rho_6 = 0, \\ e_1\rho_2 - \alpha_1{}^\alpha\rho_3 - \alpha_2{}^\alpha\rho_4 - \alpha_3{}^\alpha\rho_5 = 0, \\ -\mathcal{A}_1\rho_1 + \mathcal{A}_1\rho_2 + e_2\rho_3 - \omega^\alpha\rho_4 - \lambda^\alpha\rho_5 = 0, \\ -\mathcal{A}_2\rho_1 + \mathcal{A}_2\rho_2 + e_3\rho_4 - \theta^\alpha\rho_5 = 0, \\ -\gamma_2{}^\alpha\rho_1 + e_4\rho_5 - \gamma_1{}^\alpha\rho_6 = 0, \\ \mu^\alpha\rho_6 = 0. \end{cases}$$

After a simple calculation, we can obtain

$$\begin{aligned} &\tau_1 = q_1\tau_3,\ \tau_2 = q_2\tau_3,\ \tau_3 = \tau_3 > 0,\ \tau_4 = q_3\tau_3,\ \tau_5 = q_4\tau_3,\ \tau_6 = q_5\tau_3. \\ &\rho_1 = 0,\ \rho_2 = \rho_2 > 0,\ \rho_3 = q_6\rho_2,\ \rho_4 = q_7\rho_2,\ \rho_5 = 0,\ \rho_6 = 0. \end{aligned} \tag{4.12}$$

where

$$\begin{aligned} &q_1 = \frac{\gamma_2{}^\alpha\frac{e_2}{\alpha_1{}^\alpha} - \frac{e_1e_2}{\alpha_1{}^\alpha}}{\mathcal{A}_3},\ q_2 = \frac{e_2}{\alpha_1{}^\alpha},\ q_3 = \frac{\omega^\alpha}{e_3} + \frac{\alpha_2{}^\alpha e_2}{\alpha_1{}^\alpha e_3},\ q_4 = \frac{\alpha_3{}^\alpha e_2}{\alpha_1{}^\alpha e_4} + \frac{\lambda^\alpha}{e_4} + \frac{q_1\theta^\alpha}{e_4}, \\ &q_5 = \frac{1}{\mu^\alpha}(\delta^\alpha q_3 + \gamma_1{}^\alpha q_2),\ q_6 = -\frac{\mathcal{A}_1}{e_2} - \frac{\mathcal{A}_2\omega^\alpha}{e_2e_3},\ q_7 = -\frac{\mathcal{A}_1}{e_2}. \end{aligned}$$

Next, according to Sotomayor's theorem [58], we apply to the fractional order system to obtain:

$$\Delta_1 = (\rho_1,\ \rho_2,\ \rho_3,\ \rho_4,\ \rho_5,\ \rho_6)(0,0,0,0,0,0)^T = 0;$$

$$\Delta_2 = (\rho_1,\rho_2,\rho_3,\rho_4,\rho_5,\rho_6)\begin{pmatrix} 0 & 0 & -\mathcal{B}_1 & 0 & 0 & 0 \\ 0 & 0 & \mathcal{B}_1 & 0 & 0 & 0 \\ 0 & 0 & 0 & 0 & 0 & 0 \\ 0 & 0 & 0 & 0 & 0 & 0 \\ 0 & 0 & 0 & 0 & 0 & 0 \\ 0 & 0 & 0 & 0 & 0 & 0 \end{pmatrix}(\tau_1,\tau_2,\tau_3,\tau_4,\tau_5,\tau_6)^T$$

$$= \tau_3\rho_2\mathcal{B}_1 > 0;$$

$$
\begin{aligned}
\Delta_3 &= (\rho_1,\rho_2,\rho_3,\rho_4,\rho_5,\rho_6)[\mathcal{J}^{*2}(NAE)(\tau,\tau)]\\
&= (\rho_1,\rho_2,\rho_3,\rho_4,\rho_5,\rho_6)(2\tau_1\tau_3\begin{pmatrix} -{\beta_1}^{\alpha}{\sigma_1}^{\alpha} \\ {\beta_1}^{\alpha}{\sigma_1}^{\alpha} \\ 0 \\ 0 \\ 0 \\ 0 \end{pmatrix} + 2\tau_1\tau_4\begin{pmatrix} -{\beta_2}^{\alpha}{\sigma_2}^{\alpha} \\ {\beta_2}^{\alpha}{\sigma_2}^{\alpha} \\ 0 \\ 0 \\ 0 \\ 0 \end{pmatrix} + {\tau_3}^2\begin{pmatrix} 2a{\beta_1}^{\alpha}{\sigma_1}^{\alpha}S^0 \\ -2a{\beta_1}^{\alpha}{\sigma_1}^{\alpha}S^0 \\ 0 \\ 0 \\ 0 \\ 0 \end{pmatrix} + {\tau_4}^2\begin{pmatrix} 2b{\beta_2}^{\alpha}{\sigma_2}^{\alpha}S^0 \\ -2b{\beta_2}^{\alpha}{\sigma_2}^{\alpha}S^0 \\ 0 \\ 0 \\ 0 \\ 0 \end{pmatrix})\\
&= 2\tau_1\tau_3{\beta_1}^{\alpha}{\sigma_1}^{\alpha} + 2\tau_1\tau_4{\beta_2}^{\alpha}{\sigma_2}^{\alpha} - 2a{\beta_1}^{\alpha}{\sigma_1}^{\alpha}S^0{\tau_3}^2 - 2b{\beta_2}^{\alpha}{\sigma_2}^{\alpha}S^0{\tau_4}^2\\
&= 2\tau_3{\beta_1}^{\alpha}{\sigma_1}^{\alpha}(\tau_1 - aS^0\tau_3) + 2{\beta_2}^{\alpha}{\sigma_2}^{\alpha}\tau_4(\tau_1 - bS^0\tau_4),
\end{aligned}
$$

where $\mathcal{B}_1 = \alpha{\beta_1}^{\alpha-1}{\sigma_1}^{\alpha}\frac{\Pi^{\alpha}}{\mu^{\alpha}+\delta^{\alpha}}$. The above calculations lead us to the following theorem.

Theorem 4.4. *When ${\beta_1}^{\alpha} = {\beta_1}^{\alpha*}$, and $\tau_1 \neq aS^0\tau_3, bS^0\tau_4$ hold, the model (3.1) undergoes forward (transcritical) bifurcation at $R_0 = 1$.*

Remark 4.2. *We find that the introduced nonlinear propagation rate and the addicted population have an important role in changing the dynamical behavior of the FOSMA model (3.1). Also, the occurrence of forward bifurcation at $R_0 = 1$ is consistent with the findings in [27]. In this paper, we give a detailed proof.*

Remark 4.3. *The central manifold theorem for integer order models was utilized in [56], and Xu et al. extended the reference to the central manifold theorem to fractional order systems in [57]. We generalize the integer order Sotomayor theorem in [58, 59] to fractional order systems in our proof. This has important implications for the study of bifurcation phenomena in fractional order systems.*

5. Fractional-order sliding mode control

First, we first give partial differential models that are equivalent to fractional order systems. Then, we design the fractional order sliding mode surface of the control system. Finally, the fractional order sliding mode control law of the control system is given. To simplify the complexity of the control model, internal and external disturbance factors are omitted.

5.1. Frequency distributed model transformation

To establish the effectiveness of the fractional order sliding mode control, the following theorem is presented first.

The fractional-order system (3.1) could be reformulated in the following form:

$$
\begin{cases} \mathcal{D}^{\alpha}Y(t) = F(t, Y(t)) \\ Y(0) = (S(0), E(0), A(0), P(0), Q(0), R(0)) \end{cases} \tag{5.1}
$$

where $Y(t) = (S(t), E(t), A(t), P(t), Q(t), R(t)), F(t, Y(t)) = (F_1(t), F_2(t), F_3(t), F_4(t), F_5(t), F_6(t))$.

We employ the fractional-order numerical approximation technique as presented in [60]. We make the following assumption.

$$
\varphi(w,t) = \int_0^t e^{-w^2(t-\tau)}F(Y,\tau)d\tau, \tag{5.2}
$$

where $\varphi : (0, \infty) \times [0, T] \to R^n$.

Theorem 5.1. *Under the assumption (5.2), the system (5.19) can be rewritten as:*

$$\begin{cases} \frac{\partial \varphi(w,t)}{\partial t} = -w^2\varphi(w,t) + F(Y,t) \\ Y(t) = \int_0^\infty \varpi(w)\varphi(w,t)dw, \end{cases} \tag{5.3}$$

where $\varpi(w) = \frac{2\sin(\pi\alpha)}{\pi} w^{1-2\alpha}, \alpha \in (0, 1)$.

Proof. The proof of the theorem is divided into two steps.

Step 1: To prove Theorem 5.1, we first rewrite Eq (5.2) as follows:

$$\varphi(w,t) = e^{-w^2 t} \int_0^t e^{w^2\tau} F(Y,\tau)d\tau. \tag{5.4}$$

Differentiating both sides of the Eq (5.4), we obtain

$$\begin{aligned} \frac{\partial \varphi(w,t)}{\partial t} &= -w^2 e^{-w^2 t} \int_0^t e^{w^2\tau} F(Y,\tau)d\tau + e^{-w^2 t} e^{w^2 t} F(Y,t) \\ &= -w^2 \int_0^t e^{-w^2(t-\tau)} F(Y,\tau)d\tau + F(Y,t) \\ &= -w^2\varphi(w,t) + F(Y,t). \end{aligned} \tag{5.5}$$

Step 2: Utilizing the Gamma function and its properties, we obtain

$$\begin{aligned} {}_{t_0}I_t^\alpha F(Y,t) &= \frac{1}{\Gamma(\alpha)\Gamma(1-\alpha)} \int_{t_0}^t \frac{F(Y,\tau)}{(t-\tau)^{1-\alpha}} d\tau \int_0^\infty e^{-z} z^{-\alpha} dz \\ &= \frac{1}{\Gamma(\alpha)\Gamma(1-\alpha)} \int_0^\infty \int_{t_0}^t \frac{F(Y,\tau)}{(t-\tau)^{1-\alpha}} e^{-z} z^{-\alpha} d\tau dz \\ &= \frac{1}{\Gamma(\alpha)\Gamma(1-\alpha)} \int_0^\infty \int_{t_0}^t F(Y,\tau)\left(\frac{z}{t-\tau}\right)^{-\alpha} \frac{1}{t-\tau} e^{-z} d\tau dz. \end{aligned} \tag{5.6}$$

We define the variables as follows

$$z = w^2(t-\tau), \tag{5.7}$$

then $dz = 2w(t-\tau)dw$.

Substituting Eq (5.7) into Eq (5.6), we can derive

$$\begin{aligned} {}_{t_0}I_t^\alpha F(Y,t) &= \frac{2}{\Gamma(\alpha)\Gamma(1-\alpha)} \int_0^\infty \int_{t_0}^t F(Y,\tau) w^{1-2\alpha} e^{-w^2(t-\tau)} d\tau dw \\ &= \frac{2}{\Gamma(\alpha)\Gamma(1-\alpha)} \int_0^\infty w^{1-2\alpha} \int_{t_0}^t F(Y,\tau) w^{1-2\alpha} e^{-w^2(t-\tau)} d\tau dw. \end{aligned} \tag{5.8}$$

Furthermore, we can deduce

$${}_{t_0}I_t^\alpha F(Y,t) = \frac{2}{\Gamma(\alpha)\Gamma(1-\alpha)} \int_0^\infty w^{1-2\alpha}\varphi(w,t)dw, \tag{5.9}$$

where $\varpi(w) = \frac{2}{\Gamma(\alpha)\Gamma(1-\alpha)} w^{1-2\alpha} = \frac{2\sin(\alpha\pi)}{\pi} w^{1-2\alpha}$.

Equation (5.9) can be transformed into

$$ {}_{t_0}I_t^{\alpha} F(Y,t) = \int_0^{\infty} \varpi(w)\varphi(w,t)dw. \tag{5.10} $$

For system (5.19), the Caputo type fractional order integral expression for the function $Y(t)$ is identical to the R-L type (2.3), see ([52,53]) for details. We can obtain

$$ Y(t) = \mathcal{D}^{-\alpha} F(Y,t) = \int_0^{\infty} \varpi(w)\varphi(w,t)dw. \tag{5.11} $$

At this point, the proof of Theorem 5.1 is concluded.

5.2. Sliding mode control

The sliding mode controller is designed to converge the system towards NAE. The error is defined as follows:

$$ e_1(t) = S - S^0, e_2(t) = E - E^0, e_3(t) = A - A^0, e_4(t) = P - P^0, e_5(t) = R - R^0, e_6(t) = Q - Q^0. \tag{5.12} $$

Substituting the error (5.12) into the model (3.1), we obtain:

$$ \begin{aligned}
{}_0^C\mathcal{D}_t^{\alpha} e_1(t) &= \Pi^{\alpha} - \frac{\beta_1{}^{\alpha}\sigma_1{}^{\alpha}(e_3 + A^0)(e_1 + S^0)}{1 + a(e_3 + A^0)} - \frac{\beta_2{}^{\alpha}\sigma_2{}^{\alpha}(e_4 + P^0)(e_1 + S^0)}{1 + b(e_4 + P^0)} - (\mu^{\alpha} + \delta^{\alpha})(e_1 + S^0) \\
&\quad + \gamma_2{}^{\alpha}(e_5 + R^0) + u_1(t); \\
{}_0^C\mathcal{D}_t^{\alpha} e_2(t) &= \frac{\beta_1{}^{\alpha}\sigma_1{}^{\alpha}(e_3 + A^0)(e_1 + S^0)}{1 + a(e_3 + A^0)} + \frac{\beta_2{}^{\alpha}\sigma_2{}^{\alpha}(e_4 + P^0)(e_1 + S^0)}{1 + b(e_4 + P^0)} - (\alpha_1{}^{\alpha} + \alpha_2{}^{\alpha} + \alpha_3{}^{\alpha} + \mu^{\alpha})(e_2 + E^0) + u_2(t); \\
{}_0^C\mathcal{D}_t^{\alpha} e_3(t) &= \alpha_1{}^{\alpha}(e_2 + E^0) - (\mu^{\alpha} + \nu^{\alpha} + \lambda^{\alpha} + \omega^{\alpha})(e_3 + A^0) + u_3(t); \\
{}_0^C\mathcal{D}_t^{\alpha} e_4(t) &= \alpha_2{}^{\alpha}(e_2 + E^0) + \omega^{\alpha}(e_3 + A^0) - (\mu^{\alpha} + \theta^{\alpha})(e_4 + P^0) + u_4(t); \\
{}_0^C\mathcal{D}_t^{\alpha} e_5(t) &= \alpha_3{}^{\alpha}(e_2 + E^0) + \lambda^{\alpha}(e_3 + A^0) + \theta^{\alpha}(e_4 + P^0) - (\mu^{\alpha} + \gamma_1{}^{\alpha} + \gamma_2{}^{\alpha})(e_5 + R^0) + u_5(t); \\
{}_0^C\mathcal{D}_t^{\alpha} e_6(t) &= \delta^{\alpha}(e_1 + S^0) + \gamma_1{}^{\alpha}(e_5 + R^0) - \mu^{\alpha}(e_6 + Q^0) + u_6(t),
\end{aligned} \tag{5.13} $$

where, $u(t) = (u_1, u_2, u_3, u_4, u_5, u_6)^T \in R^6$ represent the sliding mode control law, Control $u(t)$ means family, school and social education, reducing exposure to social media, and promoting the dangers of social media. $e(t) = (e_1(t), e_2(t), e_3(t), e_4(t), e_5(t), e_6(t)) \in R^6$ represents the state vector of system (5.13).

Generally, the design process of sliding mode control can be divided into two steps. First, select a suitable sliding surface that can represent the required dynamic characteristics of the system. In this paper, we define a new fractional-order sliding surface based on the sliding surface proposed in [43,50].

$$ s(t) = \mathcal{D}^{\alpha-1} e + \mathcal{D}^{-1}(k_1 e + k_2 |e|^r \tanh(e)), \tag{5.14} $$

where $s(t) = (s_1, s_2, s_3, s_4, s_5, s_6)^T \in R^6$ are the sliding surfaces, and k_1, k_2, r are parameters within the sliding surface, with $k_1 > 0, k_2 > 0, 0 < r < 1$.

In (5.14), we choose the *tanh* function due to the fact that it is continuous and smooth without any discontinuity points compared to the sign functions. In addition, the *tanh* function is a nonlinear activation function that is more expressive and capable of capturing nonlinear relationships in the input data [61, 62]. Most importantly, the tanh function plays a crucial role in reducing oscillations. Figure 2 provides a comparison of various functions. Following the reference [62], we present the following lemma.

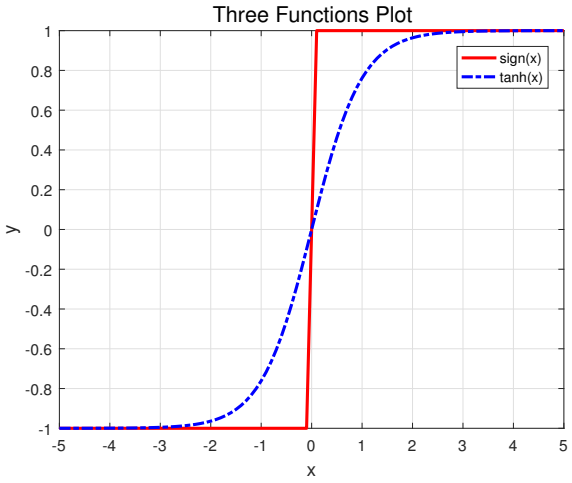

Figure 2. Graphs of the sign function, and tanh function.

Lemma 5.1. *There is a constant $j > 0$ for all $s_i \neq 0$ such that $s_i \tanh(s_i) > j s_i sign(s_i)$.*

The proof of Lemma 5.1 is detailed in [62], which we omit here. We find that using smooth continuous functions to design the controller can significantly reduce chattering.

When the system operates on the sliding surface, according to [43], it satisfies the following equation

$$s(t) = 0, \dot{s}(t) = 0. \tag{5.15}$$

Combining (5.14) and (5.15), we obtain

$$s(t) = \mathcal{D}^{\alpha-1} e + \mathcal{D}^{-1}(k_1 e + k_2 |e|^r \tanh(e)) = 0. \tag{5.16}$$

Then,

$$\mathcal{D}^{\alpha-1} e = -\mathcal{D}^{-1}(k_1 e + k_2 |e|^r \tanh(e)). \tag{5.17}$$

According to the properties of Caputo fractional order described in [52, 53], we have

$$\mathcal{D}^{\alpha} e = -(k_1 e + k_2 |e|^r \tanh(e)). \tag{5.18}$$

Theorem 5.2. *If the terminal sliding surface is chosen for the Eq (5.14), then the sliding mode system (5.18) is stable, and its state trajectories will converge to 0.*

Proof. Using the Theorem 5.1, we can transform the system (5.18) into the following equation

$$\begin{cases} \frac{\partial\varphi(w,t)}{\partial t} = -w^2\varphi(w,t) - (k_1 e + k_2|e|^r \tanh(e)) \\ e(t) = \int_0^\infty \varpi(w)\varphi(w,t)dw. \end{cases} \tag{5.19}$$

We construct a positive definite Lyapunov function

$$\mathcal{V}_1 = \frac{1}{2}\int_0^\infty \varpi(w)\varphi^2(w,t)dw. \tag{5.20}$$

Differentiating both sides of Eq (5.20), we get

$$\begin{aligned} \frac{d\mathcal{V}_1}{dt} &= \int_0^\infty \varpi(w)\varphi(w,t)\frac{\partial\varphi(w,t)}{\partial t}dw \\ &= \int_0^\infty \varpi(w)\varphi(w,t)(-w^2\varphi(w,t) - (k_1 e + k_2|e|^r \tanh(e)))dw \\ &= -\int_0^\infty \varpi(w)w^2\varphi^2(w,t)dw - \int_0^\infty \varpi(w)\varphi(w,t)(k_1 e + k_2|e|^r \tanh(e))dw \\ &= -\int_0^\infty \varpi(w)w^2\varphi^2(w,t)dw - (k_1 e + k_2|e|^r \tanh(e))\int_0^\infty \varpi(w)\varphi(w,t)dw \\ &= -\int_0^\infty \varpi(w)w^2\varphi^2(w,t)dw - (k_1 e^2 + k_2|e|^{1+r} \tanh(e)). \end{aligned} \tag{5.21}$$

According to the properties of the tanh function, when $t > 0$, $tanh(t) > 0$. Therefore,

$$\frac{d\mathcal{V}_1}{dt} < 0. \tag{5.22}$$

By applying the Lyapunov stability theory, we can conclude that the error signal in the sliding mode dynamics system (5.18) will locally asymptotically converge to 0, thus completing the proof.

After finalizing the sliding surface design, the subsequent task is to design the control input. This is to assure that the error signal reaches the sliding surface and remains on it continuously. The sliding mode control law is given as follows:

$$u(t) = -(f(e) + k_1 e + k_2|e|^r \tanh(e) + \eta_1 s + L|s|^\vartheta sign(s) + k_3 \tanh(s)), \tag{5.23}$$

where $f(e) = (f_1(e), f_2(e), f_3(e), f_4(e), f_5(e), f_6(e))$, $\eta_1, k_3, L, \vartheta$ are positive parameters with $\eta_1 > 0$, $L > 0$, (Adaptive law coefficients) $0 < \vartheta < 1$, $k_3 > 0$. Then,

Theorem 5.3. *For a given error dynamics system (5.13) and sliding surface (5.16), when the system (5.13) is subjected to the control law (5.23), the error signal of the system (5.13) will converge to the sliding surface $s(t) = 0$ within a finite duration.*

Proof. Constructing a Lyapunov function $\mathcal{V}_2(t) = |s|$ and differentiating it with respect to t, we obtain

$$\dot{\mathcal{V}_2}(t) = sign(s)\,\dot{s}\,. \tag{5.24}$$

Differentiating Eq (5.24), we obtain

$$\dot{s} = \mathcal{D}^{\alpha} e + (k_1 e + k_2 |e|^r \tanh(e)). \tag{5.25}$$

Substituting Eq (5.25) into Eq (5.24), Eq (5.24) can be rewritten as

$$\begin{aligned} \dot{\mathcal{V}_2}(t) &= sign(s)(\mathcal{D}^{\alpha} e + (k_1 e + k_2 |e|^r \tanh(e))) \\ &= sign(s)(f(e) + u(t) + (k_1 e + k_2 |e|^r \tanh(e))). \end{aligned} \tag{5.26}$$

Introducing the control law (5.23), we obtain

$$\dot{\mathcal{V}_2}(t) = sign(s)(f(e) + (-(f(e) + k_1 e + k_2 |e|^r \tanh(e) + \eta_1 s + L|s|^{\vartheta} sign(s) + k_3 \tanh(s))) + (k_1 e + k_2 |e|^r \tanh(e))). \tag{5.27}$$

Based on $s \times sign(s) = |s|$ and $sign(s) \times sign(s) = 1$, after simple calculation, we have

$$\begin{aligned} \dot{\mathcal{V}_2}(t) &= sign(s)(-\eta_1 s - L|s|^{\vartheta} sign(s) - k_3 \tanh(s)) \\ &= -\eta_1 |s| - L|s|^{\vartheta} - k_3 \tanh(s) sign(s). \end{aligned} \tag{5.28}$$

According to $\tanh(s) \times sign(s) \geq 0$, we obtain

$$\dot{\mathcal{V}_2}(t) \leq 0. \tag{5.29}$$

Based on the Lyapunov stability theory, the error signal in the error system (5.13) locally asymptotically converges to $s(t) = 0$.

From Eq (5.28) we have:

$$\begin{aligned} \dot{\mathcal{V}_2}(t) &\leq -\eta_1 |s| - L|s|^{\vartheta} - k_3 \tanh(s) sign(s) \\ &\leq -\eta_1 |s| - L|s|^{\vartheta}. \end{aligned} \tag{5.30}$$

To substitute $\mathcal{V}_2(t) = |s|$ into Eq (5.30)

$$\frac{d\mathcal{V}_2}{dt} = \frac{d|s|}{dt} \leq -\eta_1 |s| - L|s|^{\vartheta}. \tag{5.31}$$

Simplify Eq (5.31)

$$dt \leq \frac{-d|s|}{\eta_1 |s| + L|s|^{\vartheta}} = \frac{1}{\eta_1 |s|^{1-\vartheta} + L} \frac{-d|s|}{|s|^{\vartheta}} = \frac{1}{\eta_1 |s|^{1-\vartheta} + L} \frac{-d|s|^{1-\vartheta}}{1-\vartheta}. \tag{5.32}$$

Integrate both sides of Eq (5.32)

$$\int_0^{t_F} dt \leq \int_{s(0)}^{s(t_F)} \frac{1}{\eta_1 |s|^{1-\vartheta} + L} \frac{-d|s|^{1-\vartheta}}{1-\vartheta}. \tag{5.33}$$

Calculate the result for Eq (5.33)

$$t_F \leq \frac{1}{\eta_1 (1-\vartheta)} \ln\left(\frac{\eta_1 |s(0)|^{1-\vartheta} + L}{L}\right). \tag{5.34}$$

At this point, we have demonstrated that the sliding mode surface converges to $s(t) = 0$ within a finite duration.

Therefore, we can maintain the equilibrium point of the FOSMA model (3.1) around the NAE at all times by applying fractional-order sliding mode control, which serves the purpose of eliminating addiction.

5.3. Convergence-time analysis

The convergence time of stable sliding mode control can be finite or infinite. The factors that usually affect the convergence time are: the dynamic behavior of the model, the control law, or the initial conditions. Here we briefly discuss the convergence time. Assuming the system has reached a steady state, $S = 0$. To calculate the convergence time of the sliding surface, the sliding surface (5.16) is linearized near the equilibrium point ($e = 0$).

$$(\mathcal{D}^{\alpha-1} + \mathcal{D}^{-1}k_1)e = 0. \tag{5.35}$$

To determine the eigenvalues of system (5.35), we apply the Laplace transform to both sides of Eq (5.35), yielding:

$$S^{\alpha-1}E(s) - s^{\alpha-2}e(0) + k_1 \cdot \frac{1}{s}E(s) = 0, \tag{5.36}$$

where $E(s)$ is the Laplace transform of $e(t)$. Equation (5.36) simplifies to:

$$E_{(s)} = \frac{s^{\alpha-1}(0)}{s^{\alpha} + k_1}. \tag{5.37}$$

Taking the inverse Laplace transform of Eq (5.37) and simplifying, we obtain:

$$e(t) = e(0)E_{\alpha}\left(-k_1 t^{\alpha}\right). \tag{5.38}$$

Hence, the characteristic equation is:

$$E_{\alpha}\left(-k_1 t^{\alpha}\right) = 0. \tag{5.39}$$

Based on reference [62], it is observed that the convergence time is dependent on the fractional order α and the constant k_1.

Remark 5.1. *Generally, the larger the fractional order α, the slower the convergence, and the larger the k_1 value, the faster the convergence. In reference [62], the convergence time of the sliding surface dynamic attractor is calculated using a simple first-order differential equation; see reference [62] for a detailed explanation.*

6. Numerical simulation

First, we analyze the influence of key parameters in the FOSMA model (3.1) on the basic reproduction number. Then, the power series expansion method [54] will be used to numerically simulate the FOSMA model (3.1) to verify the correctness of the conclusions in Sections 4 and 5.

6.1. Effect of key parameters

First, the parameters in model (3.1) are detailed in Table 2. To study the influence of the fractional order α, the propagation rates β_1 and β_2, and the parameters ω and θ on the basic reproduction number R_0, we will use pseudo-color plots. These plots will help visualize how changes in these parameters affect the value of R_0.

Table 2. Table of references and parameter values.

References	Parameter Values
Reference [24]	$\sigma_1 = 0.5,\ \mu = 0.25,\ \delta = 0.01,\ \nu = 0.01,\ \lambda = 0.7.$
Assumed	$\Pi = 5,\ \beta_1 = 0.01,\ a = 0.5,\ \beta_2 = 0.08,\ \sigma_2 = 0.7,\ b = 0.6,\ \gamma_2 = 0.1,\ \alpha_1 = 0.35,\ \alpha_2 = 0.15,\ \alpha_3 = 0.1,\ \theta = 0.1,\ \gamma_1 = 0.3,\ \omega = 0.2.$

The warm color scheme indicates the larger value of the R_0. Through Figure 3(a) we can find that: as ω increases and θ decreases, the R_0 increases. We can reduce transmission by decreasing the ratio of addicted to professionally operated people and increasing the conversion rate from professionally operated people to recovered people. Figure 3(b), (c) shows that the basic regeneration number R_0 increases as the value of the fractional order α increases. This indicates that the basic regeneration number of our modified model (3.1) is related to the fractional order. In the real addiction propagation process, the memory effect of fractional order α significantly impacts addiction formation. After the same analysis, Figures 4 and 5 show that we can reduce the spread rate by decreasing the contact with addicted and professionally operated people to reduce large-scale addiction. Also, the value of fractional order α is important for social media addiction.

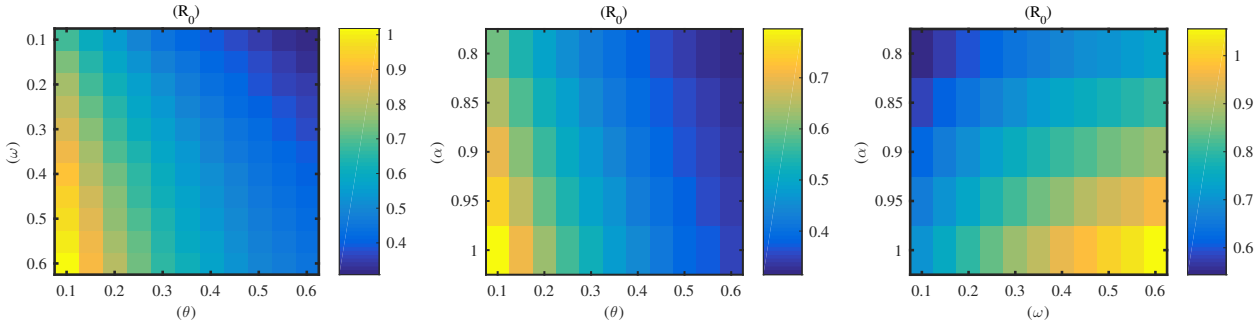

(a) (b) (c)

Figure 3. The effect of ω, θ, and α on the basic regeneration number, respectively.

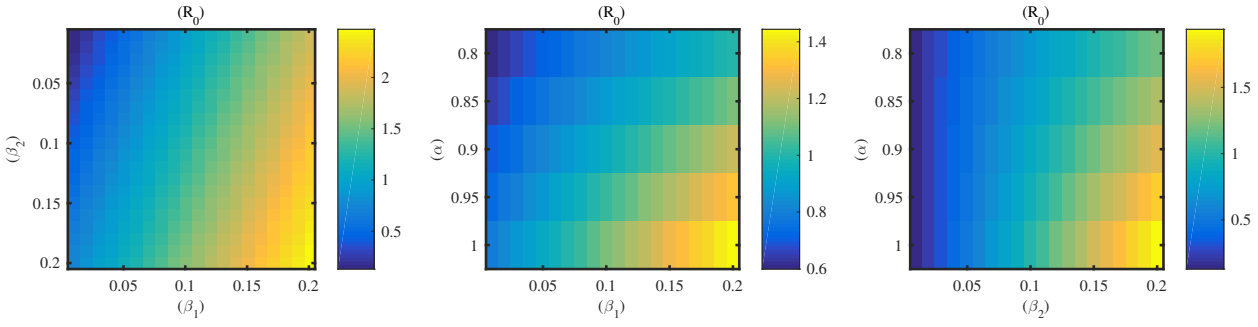

(a) (b) (c)

Figure 4. The effect of β_1, β_2, and α on the basic regeneration number, respectively.

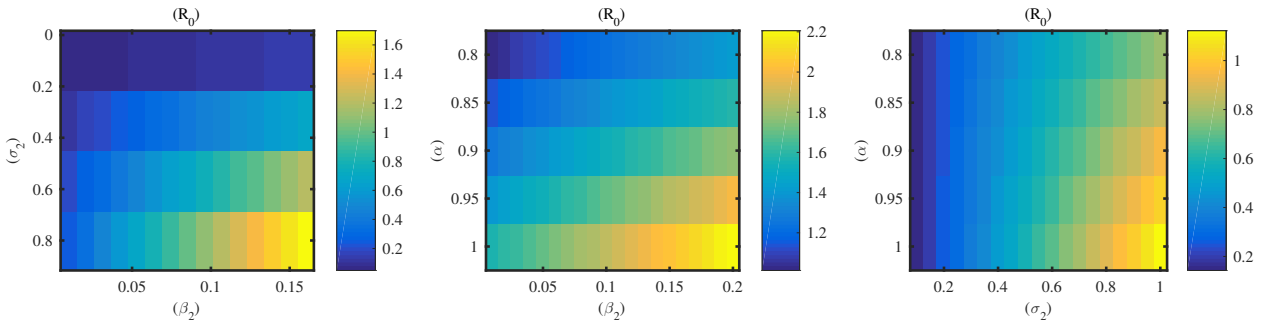

(*a*) (*b*) (*c*)

Figure 5. The effect of β_2, σ_2, and α on the basic regeneration number, respectively.

6.2. Fractional order systems

First, we keep the parameter values in model (3.1) consistent with Subsection 6.1. We choose the step size h to be 0.001. Figure 6 represents that FOSMA model (3.1) converges to NAE at different fractional order values when $R_0 < 1$.

The Figure 7 indicates that the FOSMA model (3.1) converges to AE at different fractional order values when $R_0 > 1$. Table 3 presents the data we used and shows the different results.

Table 3. Stability analysis under different parameters.

Parameter values	R_0	Stability
$\Pi = 5, S(0) = 1500, E(0) = 100, A(0) = 80, P(0) = 50, R(0) = 20, Q(0) = 50$	$R_0 < 1$	Stable
$\Pi = 20, S(0) = 1500, E(0) = 200, A(0) = 100, P(0) = 50, R(0) = 20, Q(0) = 50$	$R_0 > 1$	Stable

In the Figures 6 and 7, it can be seen from (a) that the convergence rate of the susceptible population increases as the fractional order value decreases. Panels (b) to (f) show that, with a decrease in the fractional order value, the peaks of initial exposure population, addiction population, professional operation population, recovery population and quit population all decrease, and the final convergence speed gradually increases. This shows that fractional order values significantly impact the convergence rate and peak value of the model (3.1). This also reflects the memory effect of fractional order. This is consistent with the conclusions in [63, 64].

We choose FOSMA model (3.1) parameters and initial conditions respectively $\Pi = 10$, $\beta_1 = 0.7$, $\sigma_1 = 0.8$, $\beta_2 = 0.9$; $S(0) = 1000$; $E(0) = 10$; $A(0) = 50$; $P(0) = 20$; $R(0) = 0$; $Q(0) = 100$. The other parameter values are consistent with the subsection 6.1. Moreover, we keep the numerical value of the fractional order fixed at 0.96. From Figures 8 and 9, we can find that as the saturation parameter (a, b) increases, the rate of convergence of the susceptible population slows down, and the peaks of the exposed, addicted, professionally operated, recovered, and quit populations decrease. This suggests that the nonlinear incidence in the FOSMA model (3.1) has an inhibitory or psychological effect, which would inhibit the widespread spread of addiction.

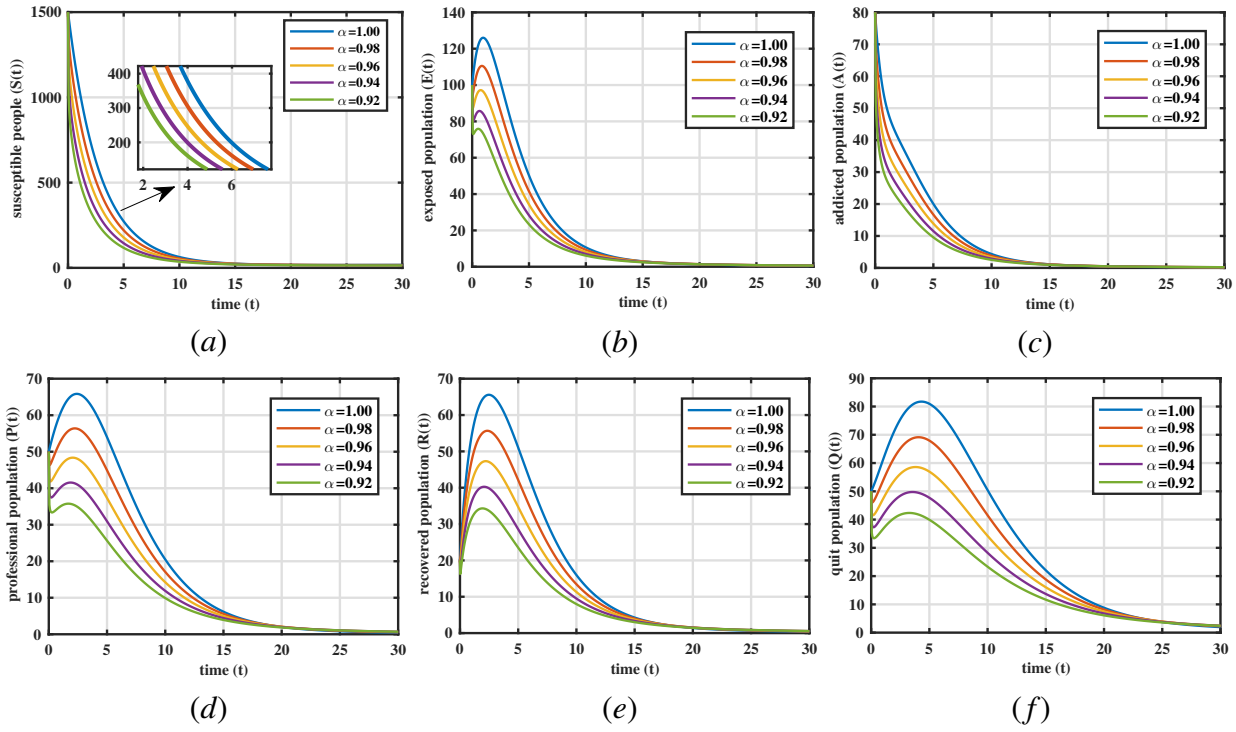

Figure 6. Plot of the trajectories of $S(t)$, $E(t)$, $A(t)$, $P(t)$, $Q(t)$, $R(t)$ at $\alpha = 1.00, 0.98, 0.96, 0.94, 0.92$ when $R_0 < 1$.

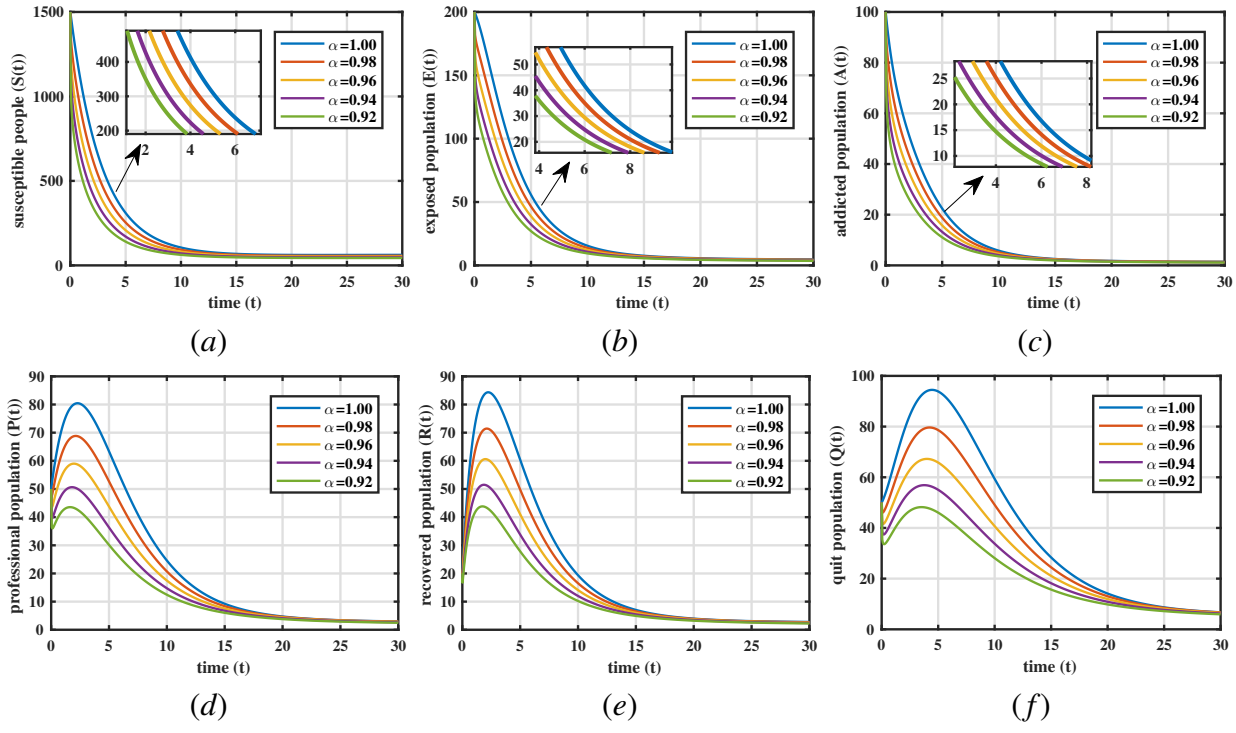

Figure 7. Plot of the trajectories of $S(t)$, $E(t)$, $A(t)$, $P(t)$, $Q(t)$, $R(t)$ at $\alpha = 1.00, 0.98, 0.96, 0.94, 0.92$ when $R_0 > 1$.

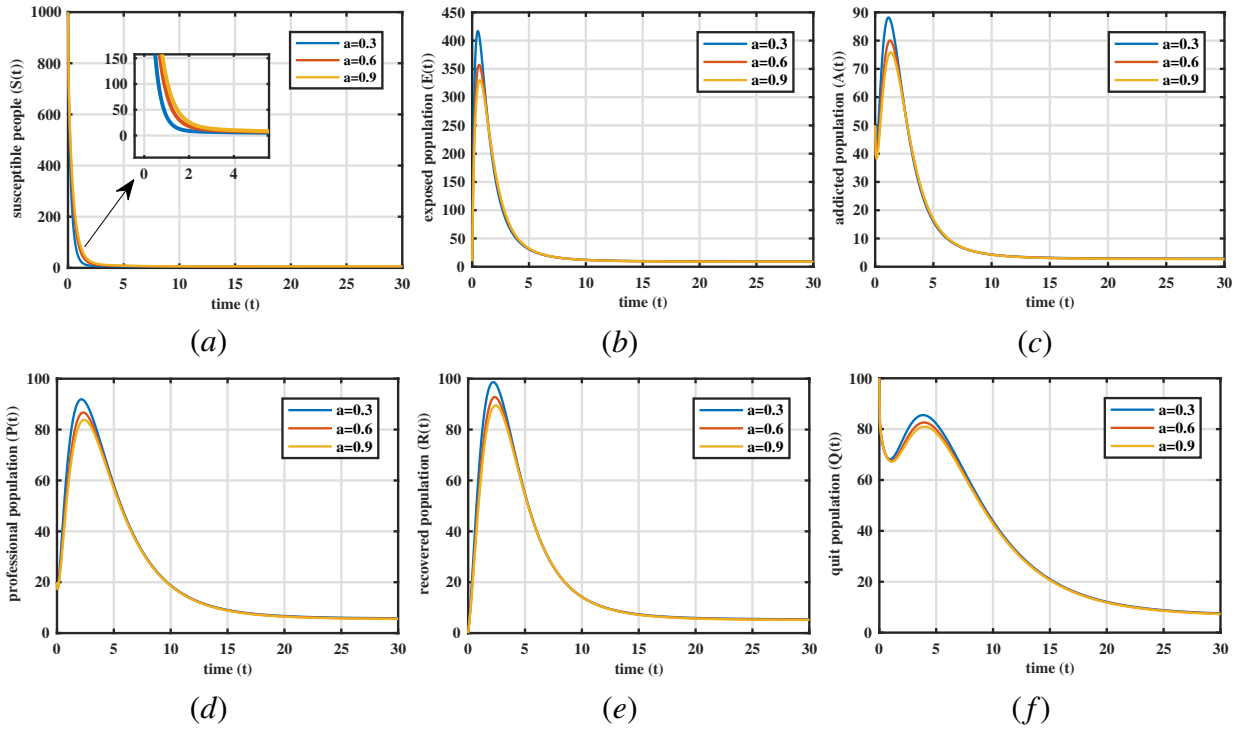

Figure 8. When $\alpha = 0.96$, a is chosen as: $0.3, 0.6, 0.9$, the trajectory of the FOSMA model (3.1) state vector.

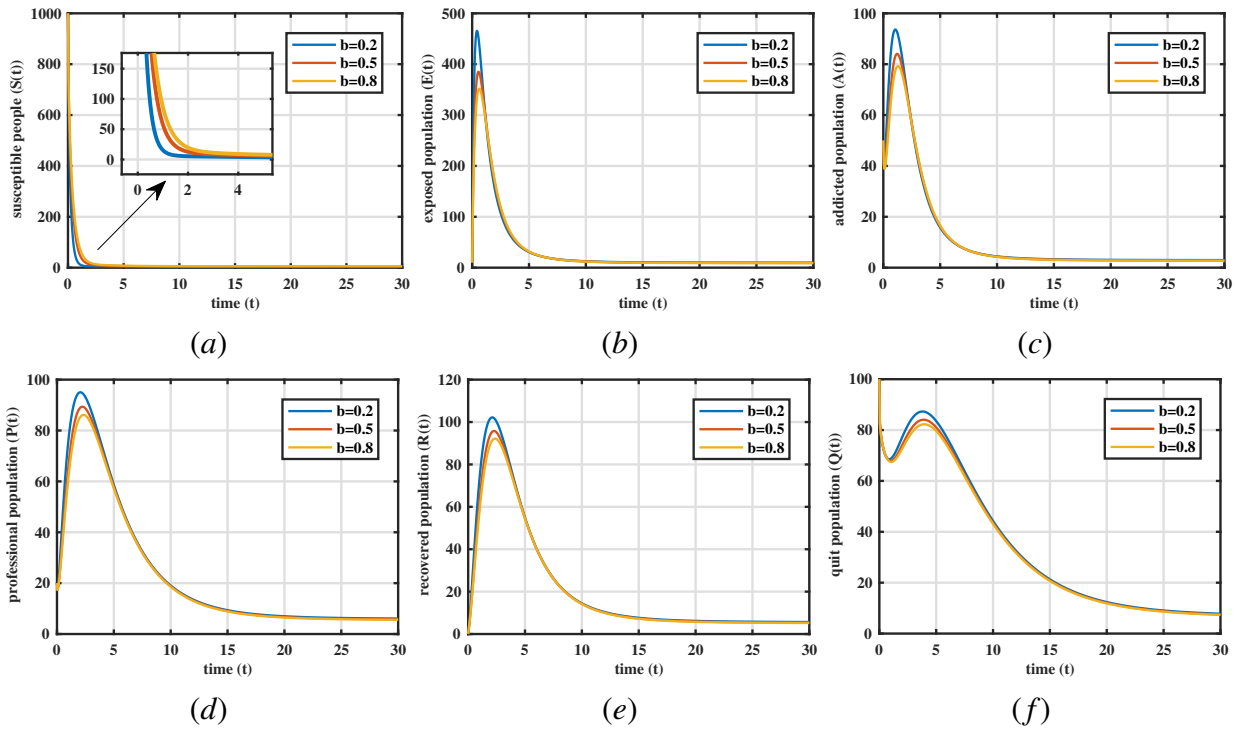

Figure 9. When $\alpha = 0.96$, b is chosen as: $0.2,\ 0.5,\ 0.8$, the trajectory of the FOSMA model (3.1) state vector.

6.3. The application of sliding mode control

We choose the parameter values of the model (3.1) to be consistent with the case $R_0 > 1$ in the Subsection (6.1). The initial conditions for the control system (5.13) are $e(0) = (25, 12, 15, 14, 10, 16)$. The initial conditions for the sliding mode surface system (5.14) is $s(0) = (10, 8, 12, 8, 9, 10)$. The initial condition for the control input (5.23) is $u(0) = (11, 14, 12, 13, 9, 14)$. We respectively choose the values of the fractional order to be 0.96 and 0.90. According to (5.14) and (5.23), we choose the gain parameters as $k_1 = 0.8, k_2 = 0.5, k_3 = 1, r = 0.5, L = 1.5, \vartheta = 0.6, \eta_1 = 1$ and a step size of $h = 0.01$, then the sliding mode surface and the control law are shown as follows:

$$s_j(t) = D^{\alpha-1}e_j + D^{-1}(0.8e_j + 0.5\left|e_j\right|^{0.5}\tanh(e_j)),$$
$$u_j(t) = -(f_j(e) + 0.8e_j + 0.5\left|e_j\right|^{0.5}\tanh(e_j) + s_j + 1.5\left|s_j\right|^{0.6}sign(s_j) + \tanh(s_j)),\ \ j = 1, 2, 3, 4, 5, 6.$$

Figure 10 shows the response images of the fractional order sliding mode surface system at various fractional orders ($\alpha = 0.96,\ 0.90$), indicating that all sliding mode surfaces converge asymptotically to 0 within a finite duration. Moreover, as the fractional order decreases, the oscillation amplitude not only advances but also decreases.

Figure 11 demonstrates the response image of the error system using fractional order sliding mode control, showing that all the error signals converge asymptotically to 0 in finite time. As the fractional order value decreases, the amplitude of the error signals decreases and the time to converge to zero decreases. We find that the model (3.1) converges to NAE with the use of the controller, then the addiction phenomenon will disappear.

As depicted in Figure 12, it is evident that all control inputs converge to zero within a finite duration. Moreover, the rate of convergence of the control inputs to zero increases as the fractional order value decreases.

Table 4 shows the coordinates of the sliding surface, error signal, and sliding mode control under different fractional orders. It can be observed that the convergence speed increases as the fractional order decreases, which is consistent with the conclusion obtained in Remark 5.1.

The above numerical simulation results illustrate that the classical integer-order sliding mode control has strong chattering, while the fractional-order sliding mode control just compensates for the drawback.

Table 4. The impact of fractional order values.

Fractional order	Sliding mode surface (s_3)	Error signal (e_3)	Sliding mode control (u_3)
$\alpha = 0.96$	(9.89, 0.024)	(10.07, −0.0158)	(14.4, −0.0276)
$\alpha = 0.90$	(8.23, 0.018)	(7.67, −0.0158)	(11.12, −0.0117)

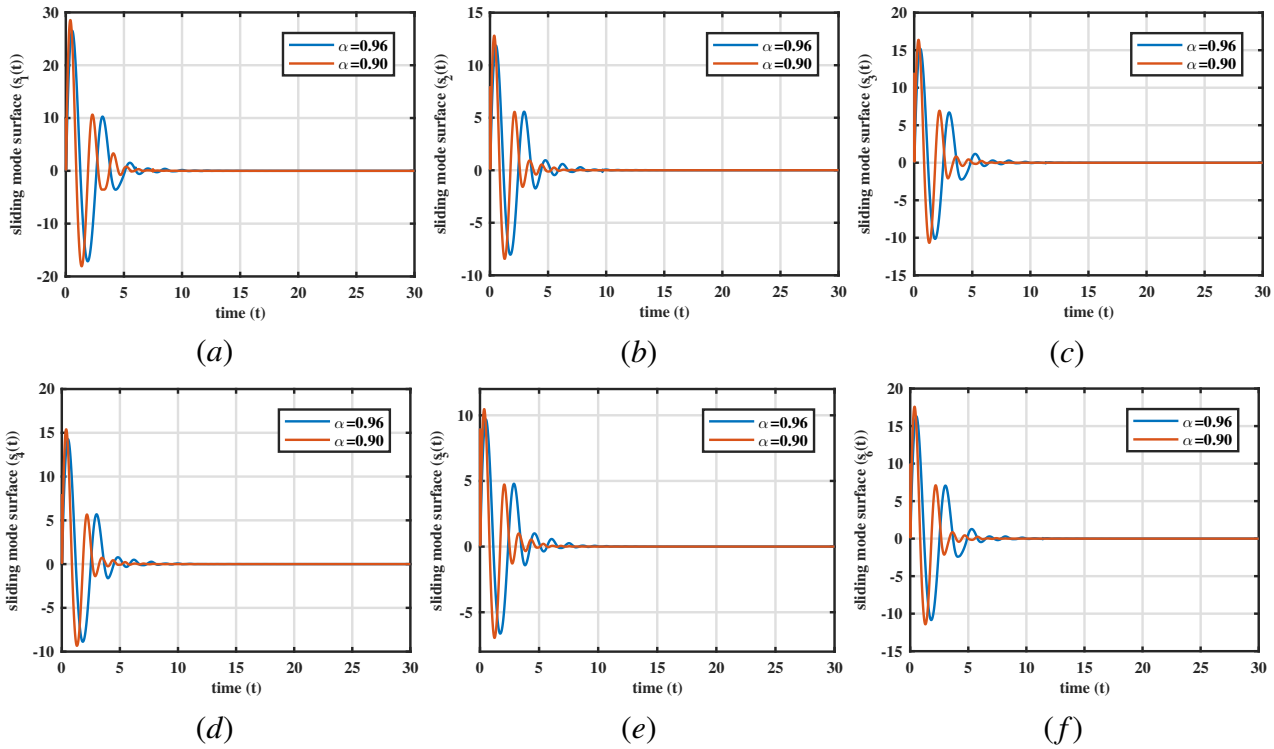

Figure 10. Fractional order sliding mode surface trajectories when $\alpha = 0.96,\ 0.90$.

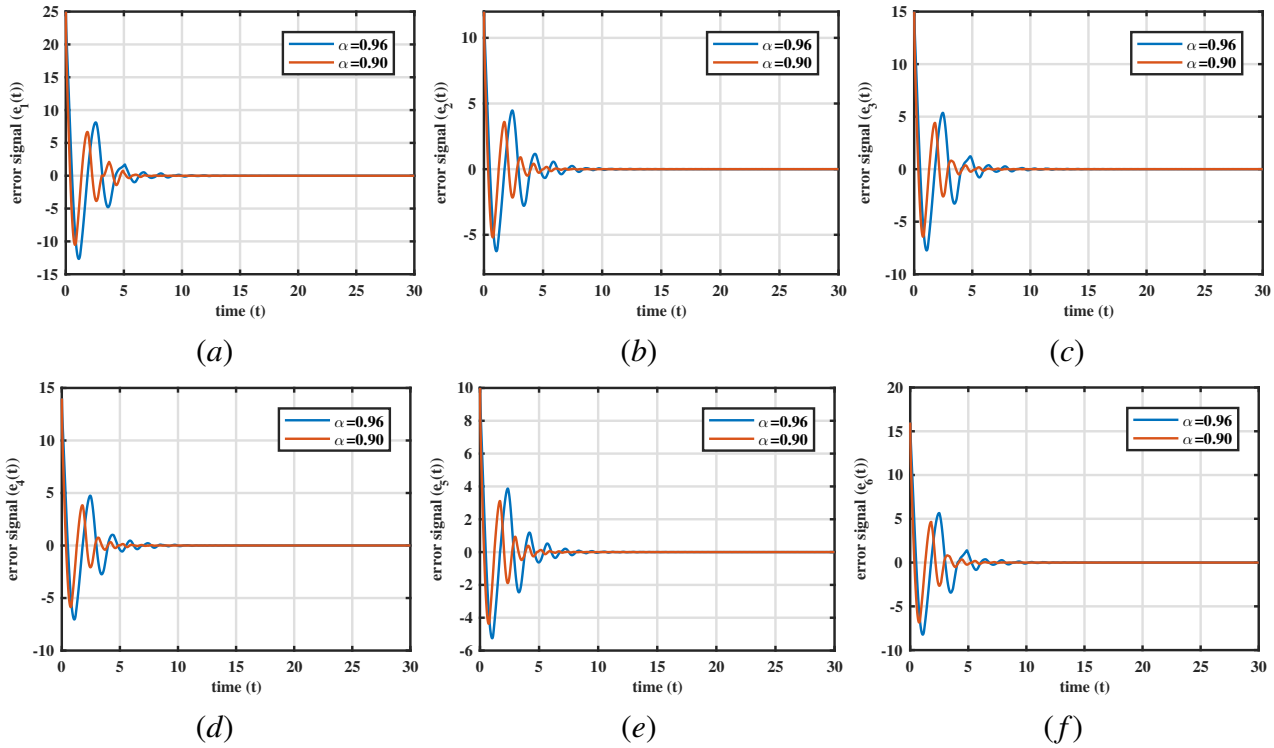

Figure 11. The trajectories of the fractional order error signaling model (5.13) when $\alpha = 0.96,\ 0.90$.

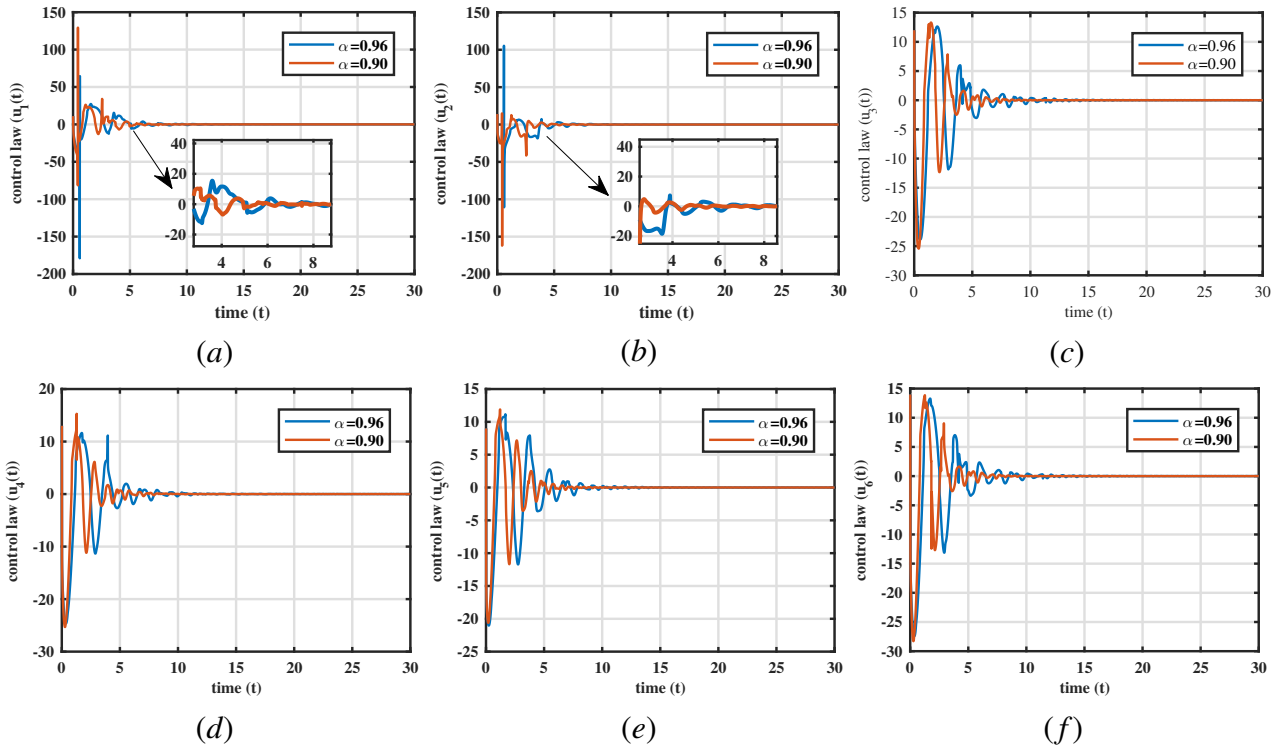

Figure 12. Trajectories of fractional order sliding mode control laws when $\alpha = 0.96,\ 0.90$.

7. Conclusions

For the first time, we include a nonlinear incidence and a professionally operating population in a modified fractional-order social media addiction model. The basic regeneration number and equilibrium points of the FOSMA model (3.1) are computed. Sufficient conditions for NAE and AE local asymptotic stability are derived. We generalize the Sotomayor theorem to fractional order systems and demonstrate the existence of forward bifurcation at $R_0 = 1$. Subsequently, the fractional order system is transformed into a partial differential model using the frequency distribution method. A fractional order sliding mode surface system is formulated, and the system's stability is demonstrated. A fractional order sliding mode control law is designed for the error signal system, demonstrating that the error signal system converges to the sliding mode surface under this control law. Finally, we find that fractional order value, propagation rate and specialized operating population have a significant effect on the basic regeneration number. Numerical simulations of the FOSMA model (3.1) reveal the importance of the fractional order value and the inhibitory factor in the nonlinear infection rate for eliminating social media addiction. With the fractional-order sliding mode control law, the error signal system will reach the sliding mode surface and further converge to 0. This also ensures that the model (3.1) will converge to the NAE, thus eliminating addiction.

In the future, we will extend our approach to modeling social media addiction to more scenarios, such as: Infectious disease modeling, ecosystem modeling, and crime modeling. Furthermore, we plan to develop a suitable fractional-order mathematical model and design fractional-order sliding mode control to address uncertainty and internal disturbances.

Use of AI tools declaration

The authors declare they have not used Artificial Intelligence (AI) tools in the creation of this article.

Conflict of interest

The authors declare there is no conflict of interest.

References

1. M. Drahošová, P. Balco, The analysis of advantages and disadvantages of use of social media in European Union, *Procedia Comput. Sci.*, **109** (2017), 1005–1009. https://doi.org/10.1016/j.procs.2017.05.446
2. L. Aburahmah, H. AlRawi, Y. Izz, L. Syed, Online social gaming and social networking sites, *Procedia Comput. Sci.*, **82** (2016), 72–79. https://doi.org/10.1016/j.procs.2016.04.011
3. F. Maclean, D. Jones, G. C. Levy, H. M. Hunter, Understanding Twitter, *Br. J. Occup. Ther.*, **76** (2013), 295–298. https://doi.org/10.4276/030802213X13706169933021
4. P. T. Ayeni, Social media sddiction: symptoms and way forward, in *The American Journal of Interdisciplinary Innovations and Research*, **1** (2019), 19–42.
5. Y. B. Hou, D. Xiong, T. L. Jiang, L. Song, Q. Wang, Social media addiction: its impact, mediation, and intervention, *Cyberpsychol. J. Psychosocial Res. Cyberspace*, **13** (2019), 4. https://doi.org/10.5817/CP2019-1-4
6. Y. Sun, Y. Zhang, A review of theories and models applied in studies of social media addiction and implications for future research, *Addict. Behav.*, **114** (2021), 106699. https://doi.org/10.1016/j.addbeh.2020.106699
7. N. Zhao, G. Zhou, COVID-19 stress and addictive social media use (SMU): mediating role of active use and social media flow, *Front. Psychiatry*, **12** (2021), 85. https://doi.org/10.3389/fpsyt.2021.635546
8. T. T. Li, Y. M. Guo, Optimal control of an online game addiction model with positive and negative media reports, *J. Appl. Math. Comput.*, **66** (2021), 599–619. https://doi.org/10.1007/s12190-020-01451-3
9. H. F. Huo, S. L. Jing, X. Y. Wang, H. Xiang, Modelling and analysis of an alcoholism model with treatment and effect of Twitter, *Math. Biosci. Eng.*, **16** (2019), 3595–3622. https://doi.org/10.3934/mbe.2019179
10. H. F. Huo, S. R. Huang, X. Y. Wang, H. Xiang, Optimal control of a social epidemic model with media coverage, *J. Biol. Dyn.*, **11** (2017), 226–243. https://doi.org/10.1080/17513758.2017.1321792
11. H. F. Huo, X. M. Zhang, Complex dynamics in an alcoholism model with the impact of Twitter, *Math. Biosci.*, **281** (2016), 24–35. https://doi.org/10.1016/j.mbs.2016.08.009

12. Y. M. Guo, T. T. Li, Fractional-order modeling and optimal control of a new online game addiction model based on real data, *Commun. Nonlinear Sci. Numer. Simul.*, **121** (2023), 107221. https://doi.org/10.1016/j.cnsns.2023.107221

13. C. T. Deressa, G. F. Duressa, Analysis of Atangana–Baleanu fractional-order SEAIR epidemic model with optimal control, *Adv. Differ. Equations*, **2021** (2021), 174. https://doi.org/10.1186/s13662-021-03334-8

14. R. Q. Shi, T. Lu, Dynamic analysis and optimal control of a fractional order model for hand-foot-mouth Disease, *J. Appl. Math. Comput.*, **64** (2020), 565–590. https://doi.org/10.1007/s12190-020-01369-w

15. N. H. Sweilam, S. M. Al-Mekhlafi, T. Assiri, A. Atangana, Optimal control for cancer treatment mathematical model using Atangana–Baleanu–Caputo fractional derivative, *Adv. Differ. Equations*, **2020** (2020), 334. https://doi.org/10.1186/s13662-020-02793-9

16. N. H. Sweilam, S. M. Al-Mekhlafi, A. O. Albalawi, Optimal control for a fractional order malaria transmission dynamics mathematical model, *Alexandria Eng. J.*, **59** (2020), 1677–1692. https://doi.org/10.1016/j.aej.2020.04.020

17. K. S. Nisar, K. Logeswari, V. Vijayaraj, H. M. Baskonus, C. Ravichandran, Fractional order modeling the Gemini virus in capsicum annuum with optimal control, *Fractal Fract.*, **6** (2022), 61. https://doi.org/10.3390/fractalfract6020061

18. H. Kheiri, M. Jafari, Stability analysis of a fractional order model for the HIV/AIDS epidemic in a patchy environment, *J. Comput. Appl. Math.*, **346** (2019), 323–339. https://doi.org/10.1016/j.cam.2018.06.055

19. C. A. K. Kwuimy, F. Nazari, X. Jiao, P. Rohani, C. Nataraj, Nonlinear dynamic analysis of an epidemiological model for COVID-19 including public behavior and government action, *Nonlinear Dyn.*, **101** (2020), 1545–1559. https://doi.org/10.1007/s11071-020-05815-z

20. P. N. Kambali, A. Abbasi, C. Nataraj, Nonlinear dynamic epidemiological analysis of effects of vaccination and dynamic transmission on COVID-19, *Nonlinear Dyn.*, **111** (2023), 951–963. https://doi.org/10.1007/s11071-022-08125-8

21. W. C. Chen, H. G. Yu, C. J. Dai, Q. Guo, H. Liu, M. Zhao, Stability and bifurcation in a predator-prey model with prey refuge, *J. Biol. Syst.*, **31** (2023), 417–435. https://doi.org/10.1142/S0218339023500146

22. K. A. N. A. Amri, Q. J. A. Khan, Combining impact of velocity, fear and refuge for the predator–prey dynamics, *J. Biol. Dyn.*, **17** (2023), 2181989. https://doi.org/10.1080/17513758.2023.2181989

23. A. Ishaku, B. S. Musa, A. Sanda, A. M. Bakoji, Mathematical assessment of social media impact on academic performance of students in higher institution, *IOSR J. Math.*, **14** (2018), 72–79.

24. H. T. Alemneh, N. Y. Alemu, Mathematical modeling with optimal control analysis of social media addiction, *Infect. Dis. Modell.*, **6** (2021), 405–419. https://doi.org/10.1016/j.idm.2021.01.011

25. B. Maayah, O. A. Arqub, Hilbert approximate solutions and fractional geometric behaviors of a dynamical fractional model of social media addiction affirmed by the fractional Caputo differential operator, *Chaos, Solitons Fractals:X*, **10** (2023), 100092. https://doi.org/10.1016/j.csfx.2023.100092
26. J. Kongson, W. Sudsutad, C. Thaiprayoon, J. Alzabut, C. Tearnbucha, On analysis of a nonlinear fractional system for social media addiction involving Atangana–Baleanu–Caputo derivative, *Adv. Differ. Equations*, **2021** (2021), 356. https://doi.org/10.1186/s13662-021-03515-5
27. S. Rashid, R. Ashraf, E. Bonyah, Nonlinear dynamics of the media addiction model using the fractal-fractional derivative technique, *Complexity* **2022** (2022). https://doi.org/10.1155/2022/2140649
28. S. M. Momani, R. P. Chauhan, D. S. Kumar, S. B. Hadid, Analysis of social media addiction model with singular operator, *Fractals* **31** (2023), 2340097. https://doi.org/10.1142/S0218348X23400972
29. P. Malik, Deepika, Stability analysis of fractional order modelling of social media addiction, *Math. Found. Comput.*, **6** (2023), 670–690. https://doi.org/10.3934/mfc.2022040
30. M. Shutaywi, Z. U. Rehman, Z. Shah, N. Vrinceanu, R. Jan, W. Deebani, et al., Modeling and analysis of the addiction of social media through fractional calculus, *Front. Appl. Math. Stat.*, **9** (2023). https://doi.org/10.3389/fams.2023.1210404
31. T. Jin, H. X. Xia, S. C. Gao, Reliability analysis of the uncertain fractional-order dynamic system with state constraint, *Math. Methods Appl. Sci.*, **45** (2022), 2615–2637. https://doi.org/10.1002/mma.7943
32. T. Jin, F. Z. Li, H. J. Peng, B. Li, D. P. Jiang, Uncertain barrier swaption pricing problem based on the fractional differential equation in Caputo sense, *Soft Comput.*, **27** (2023), 11587–11602. https://doi.org/10.1007/s00500-023-08153-5
33. I. Sen, A. Aggarwal, S. Mian, S. Singh, P. Kumaraguru, A. Datta, Worth its weight in likes: towards detecting fake likes on Instagram, in *WebSci '18: Proceedings of the 10th ACM Conference on Web Science*, (2018), 205–209. https://doi.org/10.1145/3201064.3201105
34. National Radio and Television Talent Network. Available from: http://www.nrtatalent.cn/.
35. X. Z. Li, W. S. Li, M. Ghosh, Stability and bifurcation of an SIR epidemic model with nonlinear incidence and treatment, *Appl. Math. Comput.*, **210** (2009), 141–150. https://doi.org/10.1016/j.amc.2008.12.085
36. K. Bansal, T. Mathur, S. Agarwal, Fractional-order crime propagation model with non-linear transmission rate, *Chaos, Solitons Fractals*, **169** (2023), 113321. https://doi.org/10.1016/j.chaos.2023.113321
37. H. Yuan, G. Liu, G. Q. Chen, On modeling the crowding and psychological effects in network-virus prevalence with nonlinear epidemic model, *Appl. Math. Comput.*, **219** (2012), 2387–2397. https://doi.org/10.1016/j.amc.2012.07.059
38. M. Naim, F. Lahmidi, A. Namir, A. Kouidere, Dynamics of an fractional SEIR epidemic model with infectivity in latent period and general nonlinear incidence rate, *Chaos, Solitons Fractals*, **152** (2021), 111456. https://doi.org/10.1016/j.chaos.2021.111456

39. P. L. Li, R. Gao, C. J. Xu, Y. Li, A. Akgül, D. BAleanu, Dynamics exploration for a fractional-order delayed zooplankton–phytoplankton system, *Chaos, Solitons Fractals*, **166** (2023), 112975. https://doi.org/10.1016/j.chaos.2022.112975
40. F. A. Rihan, C. Rajivganthi, Dynamics of fractional-order delay differential model of prey-predator system with Holling-type III and infection among predators, *Chaos Solitons Fractals*, **141** (2020), 110365. https://doi.org/10.1016/j.chaos.2020.110365
41. W. M. Liu, S. A. Levin, Y. Iwasa, Influence of nonlinear incidence rates upon the behavior of SIRS epidemiological models, *J. Math. Biol.*, **23** (1986), 187–204. https://doi.org/10.1007/BF00276956
42. S. G. Ruan, W. D. Wang, Dynamical behavior of an epidemic model with a nonlinear incidence rate, *J. Differ. Equations*, **188** (2003), 135–163. https://doi.org/10.1016/S0022-0396(02)00089-X
43. B. Wang, J. L. Ding, F. J. Wu, D. L. Zhu, Robust finite-time control of fractional-order nonlinear systems via frequency distributed model, *Nonlinear Dyn.*, **85** (2016), 2133–2142. https://doi.org/10.1007/s11071-016-2819-9
44. NasimUllah, A. Ibeas, M. Shafi, M. Ishfaq, M. Ali, Vaccination controllers for SEIR epidemic models based on fractional order dynamics, *Biomed. Signal Process. Control*, **38** (2017), 136–142. https://doi.org/10.1016/j.bspc.2017.05.013
45. E. E. Mahmoud, P. Trikha, L. S. Jahanzaib, O. A. Almaghrabi, Dynamical analysis and chaos control of the fractional chaotic ecological model, *Chaos, Solitons Fractals*, **141** (2020), 110348. https://doi.org/10.1016/j.chaos.2020.110348
46. C. Baishya, M. K. Naik, R. N. Premakumari, Design and implementation of a sliding mode controller and adaptive sliding mode controller for a novel fractional chaotic class of equations, *Results Control Optim.*, **14** (2024), 100338. https://doi.org/10.1016/j.rico.2023.100338
47. S. Dadra, H. R. Momeni, Control of a fractional-order economical system via sliding mode, *Physica A*, **389** (2010), 2434–2442. https://doi.org/10.1016/j.physa.2010.02.025
48. A. Boonyaprapasorn, S. Kuntanapreeda, P. S. Ngaimsunthorn, T. Kumsaen, T. Sethaput, Fractional order sliding mode controller for HBV epidemic system, *Math. Modell. Eng. Probl.*, **9** (2022), 1622–1630. https://doi.org/10.18280/mmep.090623
49. M. W. Khan, M. Abid, A. Q. Khan, G. Mustafa, M. Ali, A. Khan, Sliding mode control for a fractional-order non-linear glucose-insulin system, *IET Syst. Biol.*, **14** (2020), 223–229. https://doi.org/10.1049/iet-syb.2020.0030
50. A. Pourhashemi, A. Ramezani, M. Siahi, Dynamic fractional-order sliding mode strategy to control and stabilize fractional-order nonlinear biological systems, *IETE J. Res.*, **68** (2022), 2560–2570. https://doi.org/10.1080/03772063.2020.1719909
51. M. Borah, D. Das, A. Gayan, F. Fenton, E. Cherry, Control and anticontrol of chaos in fractional-order models of Diabetes, HIV, Dengue, Migraine, Parkinson's and Ebola virus diseases, *Chaos, Solitons Fractals*, **153** (2021), 111419. https://doi.org/10.1016/j.chaos.2021.111419
52. I. Petráš, *Fractional-Order Nonlinear Systems Modeling, Analysis and Simulation*, Springer Science & Business Media, 2011.
53. D. Baleanu, K. Diethelm, E. Scalas, J. Trujillo, *Fractional Calculus: Models and Numerical Methods*, World Scientific, 2012.

54. S. Arora, T. Mathur, K. Tiwari, A fractional-order model to study the dynamics of the spread of crime, *J. Comput. Appl. Math.*, **426** (2023), 115102. https://doi.org/10.1016/j.cam.2023.115102

55. H. M. Ali, I. G. Ameen, Stability and optimal control analysis for studying the transmission dynamics of a fractional-order MSV epidemic model, *J. Comput. Appl. Math.*, **434** (2023), 115352. https://doi.org/10.1016/j.cam.2023.115352

56. C. Castillo-Chavez, B. J. Song, Dynamical models of tuberculosis and their applications, *Math. Biosci. Eng.*, **1** (2004), 361–404. https://doi.org/10.3934/mbe.2004.1.361

57. C. H. Xu, Y. G. Yu, G. J. Ren, Y. Q. Sun, X. H. Si, Stability analysis and optimal control of a fractional-order generalized SEIR model for the COVID-19 pandemic, *Appl. Math. Comput.*, **457** (2023), 128210. https://doi.org/10.1016/j.amc.2023.128210

58. L. Perko, *Differential Equations and Dynamical Systems*, Springer Science & Business Media, 2013.

59. T. Das, P. K. Srivastava, Effect of a novel generalized incidence rate function in SIR model: stability switches and bifurcations, *Chaos, Solitons Fractals*, **166** (2023), 112967. https://doi.org/10.1016/j.chaos.2022.112967

60. L. X. Yuan, O. P. Agrawal, A numerical scheme for dynamic systems containing fractional derivatives, *J. Vib. Acoust.*, **124** (2002), 321–324. https://doi.org/10.1115/1.1448322

61. S. H. Rouhani, E. Abbaszadeh, M. A. Sepestanaki, S. Mobayen, C. L. Su, A. Nemati, Adaptive finite-time tracking control of fractional microgrids against time-delay attacks, *IEEE Trans. Ind. Appl.*, **60** (2024), 2153–2164. https://doi.org/10.1109/TIA.2023.3312223

62. P. C. Lin, E. Abbaszadeh, S. Mobayen, S. H. Rouhani, C. L. Su, M. H. Zarif, et al., Soft variable structure fractional sliding-mode control for frequency regulation in renewable shipboard microgrids, *Ocean Eng.*, **296** (2024), 117065. https://doi.org/10.1016/j.oceaneng.2024.117065

63. M. Sadki, S. Harroudi, K. Allali, Fractional-order SIR epidemic model with treatment cure rate, *Partial Differ. Equations Appl. Math.*, **8** (2023), 100593. https://doi.org/10.1016/j.padiff.2023.100593

64. J. Danane, K. Allali, Z. Hammouch, Mathematical analysis of a fractional differential model of HBV infection with antibody immune response, *Chaos, Solitons Fractals*, **136** (2020), 109787. https://doi.org/10.1016/j.chaos.2020.109787